Role of Lysocardiolipin AcylTransferase in Lung Epithelial Cell Apoptosis

BY

MOUNICA BANDELA
B.Tech., Chaitanya Bharati Institute of Technology, Osmania University, 2015
PG Diploma, Osmania University, 2016

THESIS

Submitted as partial fulfillment of the requirements
for the degree of Master of Science in Bioengineering
in the Graduate College of the
University of Illinois at Chicago, 2018

Chicago, Illinois

Defense Committee:

Dr. Viswanathan Natarajan, Chair and advisor, Department of Pharmacology and Medicine
Dr. Richard L. Magin, Academic advisor, Department of Bioengineering
Dr. Kamesh Bikkavilli, Pulmonary, Critical care, Sleep and Allergy/Medicine

This Thesis is dedicated to my Mom, Dad and brothers, without their support and belief in me, I would never accomplish my goals.

ACKNOWLEDGEMENTS

Firstly, I thank my mother Mrs. Jayasree Bandela, my father Mr. B. R. Jithender and brothers Kranthi Kumar and Kiran Kumar, for their constant support, love and belief in me which encouraged me every day to overcome all the struggles and achieve my goals. It gives me pleasure in expressing deep sense of gratitude and veneration for my family and friends.

I express my profound gratitude and heartfelt thanks to my advisor Dr. Viswanathan Natarajan, for all the encouragement, guidance, motivation and support extended to me during the tenure of my project. I would like to thank my thesis committee members Dr. Richard L. Magin and Dr. Kamesh Bikkavilli for their contribution for successful completion of my thesis.

I thank all the members of Dr. Natarajan's lab, Dr. Long Shuang, Dr. Anantha Harijith, Mark Shaaya and Dr. Yashaswini for their valuable insights and constant support. I thank Dr. Panfeng Fu and Dr. David Ebenezer for training me in important Molecular Biology Techniques. I specially thank Dr. Vidyani Suryadevara for her cooperation and support which instilled confidence in me to complete my thesis work. I thank Dr. Steve Dudek for the opportunity provided and his lab members for their extended friendship. I thank Lakshmi aunty for showering her love and affection. I thank Dr. Subbaiah Papasani for permitting me to use his lab equipment's, and I thank Dr. Sugasini for assisting me to perform Lipid phosphorous estimation.

I extend my gratitude for the administrative staff of Department of Bioengineering and Division of Pulmonary, Critical Care, Sleep and Allergy, for providing necessary facilities and help when required. Lastly, I would like to thank my roommates Alekhya Pujari and Shriya Saridana for their company and friendship in the United States.

Mounica Bandela

TABLE OF CONTENTS

III RESULTS

LIST OF FIGURES

LIST OF ABBREVIATIONS

COPD - Chronic Obstructive Pulmonary Disorder

CT - Computed Tomography

CDP-DAG - Cytidine diphosphate diacylglycerol

CTP - Cytidine triphosphate

MLCL - Monolysocardiolipin

CL - Cardiolipin

ALCLAT - Acyl CoA:lysocardiolipin acyltransferase

LYCAT – Lysocardiolipin acyltransferase

PDB - protein databank

NMR - Nuclear Magnetic Resonance

BLAST - Basic Local Alignment Search Tool

HPEPDOCK- Hierarchical Peptide docking

GAPDH - glyceraldehyde 3-phosphate dehydrogenase

CSE - Cigarette smoke extract

RT PCR - Real Time Polymerase chain reaction

TLC - Thin Layer Chromatography

GC-MS - Gas Chromatography-Mass spectroscopy

NCBI - National Center for Biotechnology Information

SUMMARY

Chronic Obstructive Pulmonary Disorder (COPD), primarily caused by cigarette smoke (CS), is a leading cause of mortality in the US. In the present study, we investigated the role of Lysocardiolipin acyltransferase (LYCAT), a cardiolipin remodeling enzyme in the pathogenesis of COPD, with the goal to better understand the molecular mechanisms that occur during COPD. An *in vitro* model of bronchial epithelial cells exposed to cigarette smoke extract (CSE) was employed in our study. The findings of the present study are: 1, CSE enhanced mRNA and protein expression of LYCAT; 2, CSE enhanced mitochondrial ROS generation and apoptosis in human bronchial epithelial cells; 3, Blocking LYCAT activity with a newly developed peptide mimetic reduced CSE-mediated mitochondrial ROS and apoptosis of Beas2B cells. Thus, inhibiting LYCAT expression or activity may have therapeutic role in COPD.

In vitro data suggested that modulating the expression levels of LYCAT could be a novel therapeutic approach in COPD for drug design. LYCAT 3D structure is not available in databases, therefore by using computer assisted technology, such as MODELLER9.19, a homology model was built. The template structure 1BD2 was retrieved by PDB-BLAST. The LYCAT homology model was validated for structural assessment using Ramachandran plot, QMEAN and Z-scores. There were 84.76% of residues in favored region of Ramachandran plot, and the QMEAN and Z-scores were -11.19 and -0.94 respectively. The assessed model was further refined. The biological active site of LYCAT was predicted using CASTp with 1417.854 $Å^3$ and 2029.864 $Å^2$ as the surface area and volume of the largest pocket respectively. The validated homology model was docked with the

peptide mimetic using HPEPDOCK, which gave multiple models among those, the one with lowest docking energy i.e., -251.093 $Kcalmol^{-1}$ was considered as best binding model. Having identified LYCAT as a potential target in COPD, there is need to develop novel small molecule inhibitors for further *in vivo* and *in vitro* studies

I. INTRODUCTION

Background:

Chronic obstructive pulmonary disorder (COPD) is a serious lung injury, which causes mortality worldwide. According to American Lung Association, COPD is the third leading cause of death and more than 11 million people suffer from it in the United States, but it is preventable and treatable with maintaining good symptom control and quality of life. The key for successful treatment is early detection. The primary cause for development of COPD is cigarette smoking, while other causes include long term exposure to irritating gases, particulate matter, and lung cancer.

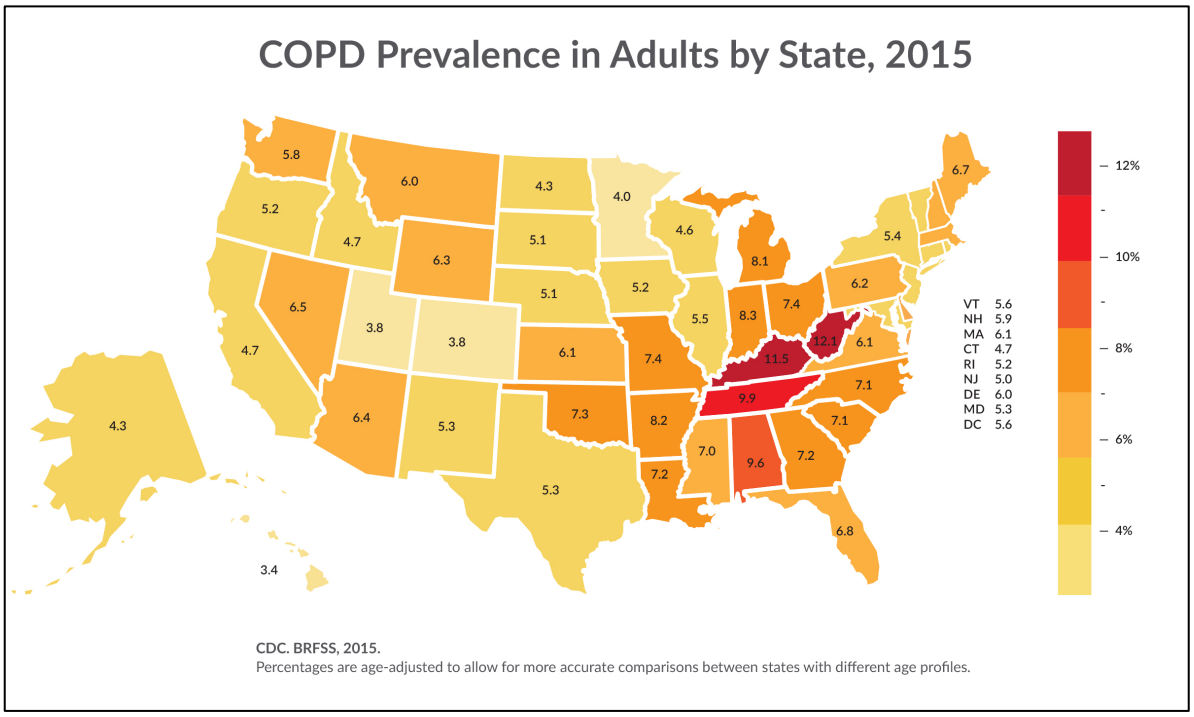

Figure 1. Epidemics of COPD in United States. Reprinted with permission from American Lung Association.©2018 from American Lung Association.

1. COPD:

a. Definition:

According to World Health Organization, COPD is defined as "Chronic obstructive pulmonary disorder" (COPD), is a lung disease characterized by chronic obstruction of lung airflow that interferes with normal breathing and is not fully reversible.

b. Etiology:

The primary risk factor for development of COPD is long term exposure to cigarette smoke, which leads to lung damage. The other factors include genetic disorder, such as Alpha-1-antitrypsin deficiency[1].

c. Mechanics of Breathing:

The main parts of lung are bronchial tubes and alveoli, and air moves through the trachea down the bronchial tubes and alveoli. Oxygen goes into blood and carbon dioxide comes out of the blood from the alveoli [2].

COPD encompasses two pulmonary illness, namely chronic bronchitis and emphysema.

In **chronic bronchitis** illness the bronchial tubes get red, swollen and filled with mucus. This leads to inflammation and narrowing of the bronchial tubes and excess mucus produced by the lungs blocks the narrowed tubes. Chronic cough is developed to clear the airways and makes hard to breathe. In **emphysema** condition, alveoli are lost and makes it hard for the movement of oxygen and carbon dioxide into and out of the blood, and therefore inhaling and exhaling becomes difficult in this condition. This causes destruction of the elastic fibers and fragile walls of the alveoli [3, 4].

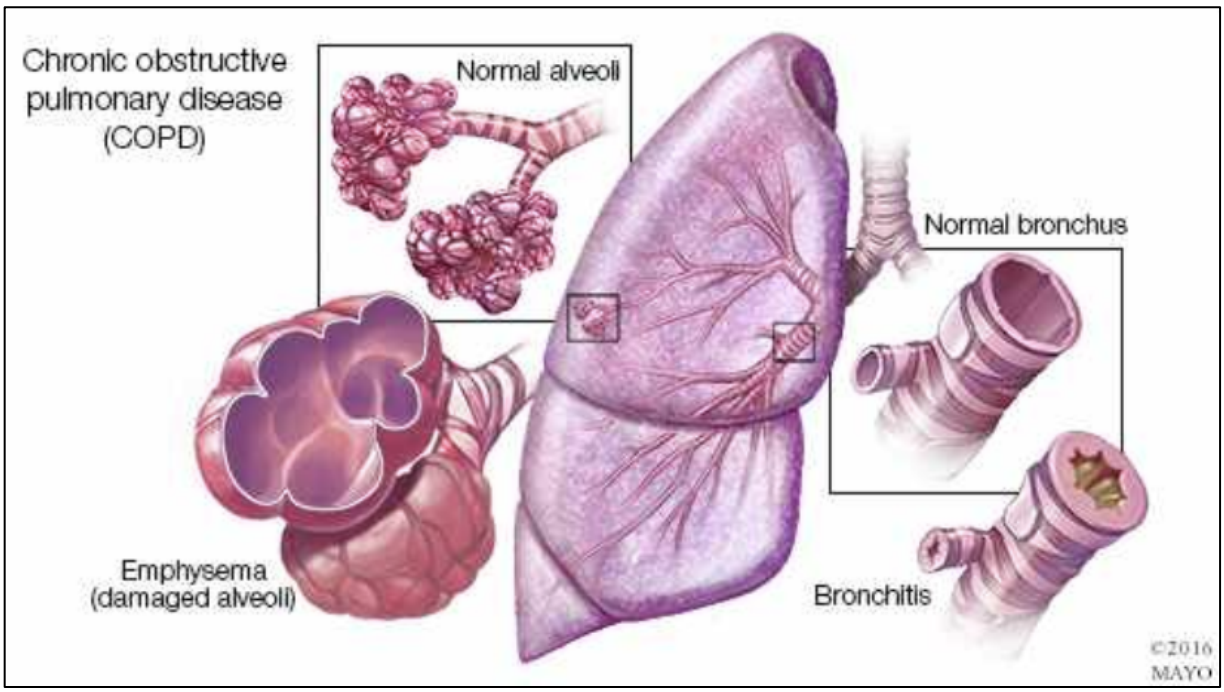

Figure 2. Chronic Bronchitis and Emphysema illness of COPD. Reprinted with permission from Mayo Clinic. © MAYO FOUNDATION FOR MEDICAL EDUCATION AND RESEARCH.

d. Symptoms of COPD:

COPD symptoms do not appear initially until lung damage occur, and it gets worsen if smoking persists. People experience exacerbations when the symptoms worsen. .

The other main symptoms of COPD are: Wheezing, Cough, Fatigue, Shortness of breath, Chest tightness, Excess Mucus, Cyanosis, Lack of Energy, Respiratory Infections, swelling of ankles, feet or legs and Weight Loss.

e. Risk Factors:

Exposure to tobacco smoke: Main risk factor is cigarette smoking. Long term exposure to tobacco smoking leads to COPD. Second hand smokers, pipe smokers and cigar smokers also have the risk.

Occupational exposure to dust and chemicals: Inflammation and irritation of airways and lungs occur due to long term exposure to industrial dust, chemicals and gases, which increases the risk of developing COPD. People who work in coal mines, grain handling and metal molding are more likely to get COPD.

Air-pollution: Prolonged exposure to intense outdoor and indoor particulate matter like smoke from burning fuel, biomass or coal, or cooking fire can also lead to COPD in developing countries. In urban countries air-pollution due to combustion or traffic can cause COPD.

Age: Even without the history of smoking people can develop COPD, its common in people above 40 years since the incidence increases with age.

Genetics: Genetic disorder can also be a factor for developing COPD. Deficiency in Alpha Antitrypsin can cause COPD.

f. Diagnosis of COPD:

According to American lung Association the methods used to diagnose COPD include-

Pulmonary function test: The risk and symptoms for COPD can be detected by simple test called spirometry. This test analyses the function of lungs and can detect COPD even before symptoms are developed. The severity of the disease can be determined to set treatment goals.

Other tests: COPD can be detected with Chest X-ray, CT scan or arterial blood gas test. Emphysema can be shown in chest X-ray or CT scan. In arterial blood gas test, oxygen level in the blood can be measured, which analyzes the exchange of gases.

Laboratory tests: Genetic disorder due to anti trypsin deficiency can be determined by laboratory tests.

g. Treatment:

Effective treatment is required to control symptoms, reduce risk of complications and exacerbations.

Smoking cessation: The disease gets exacerbated due to excessive smoking, and therefore the essential step in treatment of COPD is quitting smoking. Nicotine replacement products and medications can be used with some proven benefits. Secondhand smoking should also be avoided.

h. Medications:

Bronchodilators: Bronchodilators are prescribed to relax the muscles around the airways. Breathing can be made easier since its gives relieve from coughing and shortness of breath. Albuterol,levalbuterol,ipratropium,tiotropium,salmeterol,formoterol,indacaterol, arformoterol and aclidinium are some of the commonly prescribed bronchodilators in the US.

Inhaled steroids: Inhaled steroids like corticosteroids (budesonide and fluticasone) can reduce airway inflammation and prevents exacerbations and prescribed under certain circumstances.

Combination inhalers: Inhaled steroids and bronchodilators are given together. Salmeterol and fluticasone is an example of combination inhalers.

Phosphodiesterase-4 inhibitors: Roflumilast, is a Phosphodiesterase-4 inhibitor, which is the new drug approved for severe COPD. Airway inflammation is decreased and leads to relaxation of the airways.

Theophylline: Improves breathing and prevents exacerbations, it is an inexpensive drug.

Lung therapies: Oxygen therapy and pulmonary rehabilitation program are other therapeutic methods to improve oxygen in the blood and quality of life.

i. Surgery:

Lung volume reduction surgery: This surgery improves quality of life and prolongs survival. Extra space in the chest cavity is created by removing the small wedges of the damaged upper lung which gives sufficient space for healthy lung to expand and work efficiently.

Lung transplant: This is special criteria for certain people. It's a major operation that has risks such as organ rejection and being on immuno- suppressing medications. It improves ability to breathe and be active.

Bullectomy: Large air spaces called bullae are formed in the lungs due to air sacs destruction, which leads to breathing problems. These bullae are removed in bullectomy which improves air flow.

2. Lipids:

Lipids are fat soluble molecules that are important components of biological membranes present on the plasma membrane, mitochondrial membranes, endoplasmic reticulum, nucleus of mammalian cells. Lipids are soluble in organic solvents and insoluble in water. Plasma membrane lipids provide fluidity to the cells, constitute about 50% of the animal cell membranes, and 1μm x 1μm area of lipid bilayer has about 10^9 lipid molecules in the plasma membrane. The lipid bilayer is majorly composed of phospholipids, glycolipids and cholesterol.

a. Phospholipids:

Phospholipids are the major component of cell membrane, and are made up of fatty acids, one or more phosphate group and a one or more glycerol moiety. They form double layer which is a characteristic of biological membranes.

b. Structure of Phospholipids:

Phospholipids are made up of two long chain saturated, monounsaturated or poly unsaturated fatty acids, and a phosphate head group. The long chain fatty acids are made of carbon and hydrogen, while the phosphate consists of phosphorus attached to four oxygen molecules. These two components are connected to glycerol molecule. The phosphate group is hydrophilic in nature and fatty acids are hydrophobic in nature, this gives amphyllic property to the phospholipids. Phospholipids are selectively permeable, only certain molecules can move into and out of the cell. Phospholipids can be broken down and used as energy, and generate bioactive phospholipids, which can bind to receptors on the plasma membrane and signal to regulate various cellular activities.

c. Biosynthesis of Cardiolipin:

Bis-(1,2-diacyl-sn-glycero-3-phospho)-1′-3′-sn-glycerol or cardiolipin (CL) is the major poly-glycerophospholipid in mammalian tissues. The synthesis of phospholipids occurs in endoplasmic reticulum and later they are imported to mitochondria but cardiolipin is unique where its exclusively synthesized in mitochondria[5]. It makes up 5 % of total cellular phospholipids and ~20% of mitochondrial phospholipids. Its predominantly found in the inner membrane of mitochondria and is involved oxidative phosphorylation, electron transport chain and apoptosis. Biosynthesis of cardiolipin involves two pathways[6].

- *De novo* synthesis
- Remodeling

d. *De novo* synthesis:

Phosphatidic acid (PA) is the key intermediate for the biosynthesis of phospholipids in mammalian cells. PA is generated from glycerol-3-phosphate and acyl dihydroxyacetone phosphate and is converted to cytidine diphosphate diacylglycerol (CDP-DAG) from CTP.
In further reactions, CMP in CDP-DAG is displaced by either serine, inositol or glycerol to generate phosphatidylserine, phosphatidylinositol or 3-phosphatidyl glycerol 1'-phosphate respectively.

3-Phosphatidyl glycerol 1'-phosphate is the precursor for phosphatidyl glycerol (PG) and cardiolipin. Dephosphorylation of PG and a second condensation with CDP-DAG yields di-

phosphatidylglycerol, commonly referred to as cardiolipin (CL). The *de novo* pathway generates CL that has mostly C16:0, C18:0 and some C18:1 long chain fatty acids.

e. Remodeling of Cardiolipin:

Following the *de novo* synthesis of CL, fatty acyl chain remodeling is important for the final composition of mature CL, which refers to symmetric incorporation of unsaturated fatty acyl chains. CL is deacylated to monolyso-CL (MLCL) by CL-specific phospholipase A2, and reacylation of MLCL is accomplished by three distinct proteins; tafazzin, monolysocardiolipin acyltransferase 1 (MLCLAT1), and acyl-CoA:lysocardiolipin acyltransferase-1 (ALCAT1 or LYCAT). MLCLAT1 and ALCAT1/LYCAT utilize long-chain fatty acyl-CoA as the acyl chain donor for the reacylation of MLCL; tafazzin is a transacylase that takes an acyl chain from another phospholipid, such as phosphatidylcholine or phosphatidylethanolamine and transfers it to MLCL.

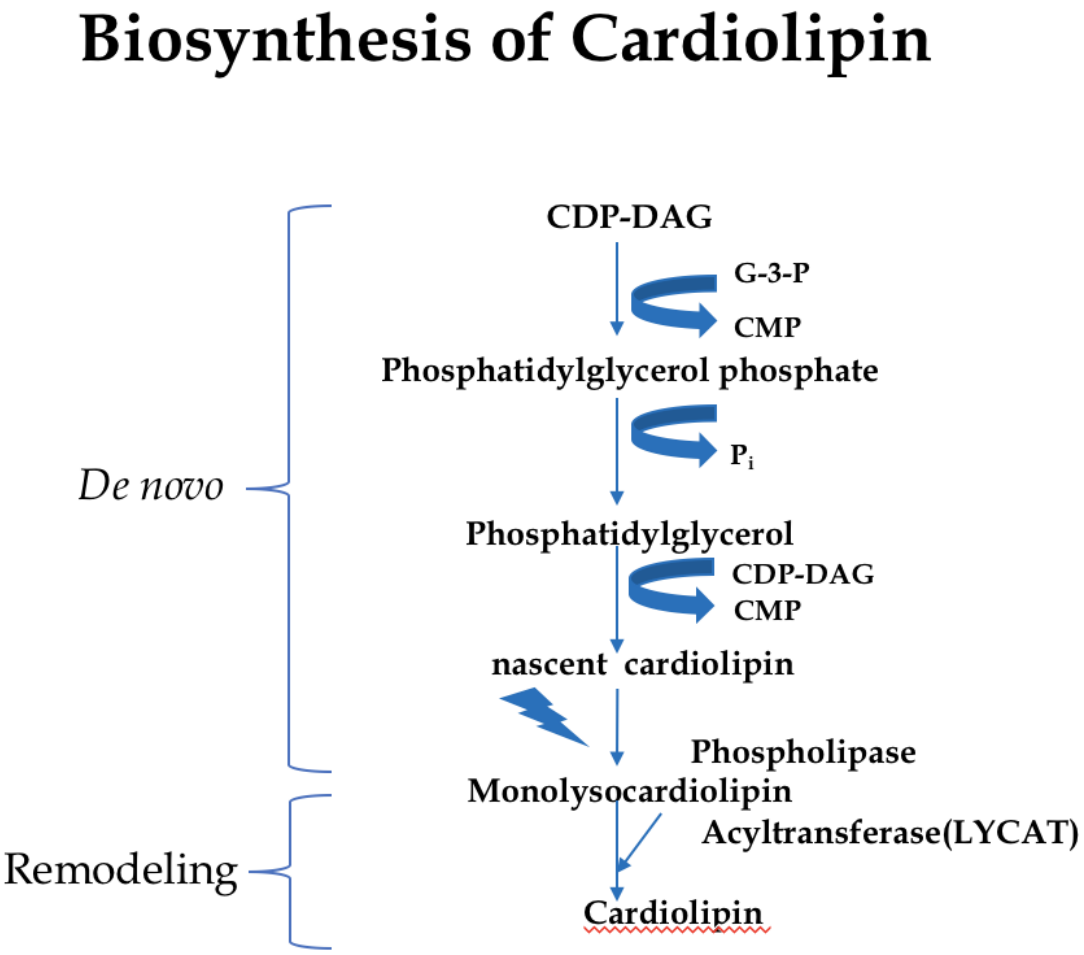

Figure 3. Biosynthesis of Cardiolipin.

3. The role of LYCAT in *in vitro* embryonic stem-cell differentiation and vascular integrity.

A study was conducted by Wang *et al* on role of mouse LYCAT on hematopoietic and endothelial lineages during *in vitro* ES cell differentiation [7]. It was demonstrated that LYCAT is the first acyltransferase essential for development of hematopoietic and endothelial in mouse embryonic stem cells. Their data shows that mouse LYCAT has the highest expression in definitive hematopoietic site called AGM region, also mRNA LYCAT is enriched in HSC's. These studies on in role of LYCAT mRNA in transduced embryonic stem cells can evaluate the LYCAT gene or protein as a potential regenerative medicine. In their further studies they worked on the role of LYCAT in angiogenesis and vascular integrity, examined temporal and spatial expression patterns of LYCAT. The data showed that expression of LYCAT was found in primitive streak, cardiogenic mesoderm and extra embryogenic mesoderm, and later expression was confined to vascular smooth muscle cells suggesting a role in angiogenesis and maintaining integrity of vasculature. LYCAT expression in embryonic mesoderm suggests that it's an important gene in hematopoietic and endothelial cell lineage and such studies provide an evidence that LYCAT gene could be responsible for the study of cloche mutant phenotypes in zebrafish [8],[7],[9].

4. The role of LYCAT in Pulmonary fibrosis:

Long *et al* showed that LYCAT protein expression is enhanced in the lung tissues from Idiopathic Pulmonary Fibrosis patients and animal models of pulmonary fibrosis[10]. Further, their study demonstrated a role for LYCAT over-expression in mitochondrial ROS, apoptosis, and cardiolipin remodeling in pulmonary fibrosis. Overexpression of human LYCAT in mice

reduced bleomycin-induced lung fibrosis, attenuated Mito-ROS, and apoptosis in epithelial cells and restored mitochondrial membrane potential [10]. This study also identified that modulation of LYCAT expression in pulmonary fibrosis can be a therapeutic approach in reducing lung inflammation and lung fibrosis [11].

Further Fu et al., reported a role of NADPH oxidase (NOX) 2 and 4 expression and oxidant production in progression of fibrosis and lung fibroblast differentiation. TGF-β induced mitochondrial superoxide production, NOX 4 expression and differentiation of human lung fibroblasts was blocked when treated with Mito-TEMPO, and by overexpressing LYCAT. This suggests that LYCAT is regulating TGF-β-induced lung fibroblast differentiation, which may serve as a therapeutic target for pulmonary fibrosis [10].

5. The role of Cardiolipin in Apoptosis:

The electron transfer from complex III to complex IV in the mitochondrial respiratory chain is mediated by cytochrome *c*. Cytochrome *c* also acts as a catalyst for peroxidation of cardiolipin, which leads to apoptosis. This increased peroxidase activity targets the polyunsaturated C18:2 fatty acids in CL, thus leading to oxidation of cardiolipin; which leads to loosing interaction between cytochrome c and oxidized CL, allowing cytochrome *c* release from mitochondria during apoptosis[4].

6. Homology Modeling:

The 3D protein structures have vast application in drug design and provide insight to study the molecular basis of protein functions, such as site directed mutagenesis, disease related mutations or design of inhibitors using structure-based drug design. The field of experimental drug design is done to identify active compounds and develop structural modifications using X-ray crystallography and nuclear magnetic resonance spectroscopy. These methods are expensive, laborious and time-consuming process with no guaranteed success. To date approximately 20,000 experimental structures developed by NMR or X-ray crystallography are deposited in the protein data bank (PDB), therefore structurally characterized proteins are low compared to the number of protein sequences available, and there are 8,50,000 sequences deposited in SWISS-PORT and TrEMBL databases together [12]. Therefore, majority of protein sequences do not have structural information, and it is important to develop 3D structures by computational methods that have gained much interest in recent years.

These *in silico* based development of 3D protein structures has advanced studies related to structure-function relationship, ligand-protein interactions, characterize binding pockets, assess the ability of drugs to bind to active sites, and optimize generation of lead compounds. Further, *in silico* methods are cheaper, faster, and efficient in drug discovery. It has been shown that 3D protein structure is evolutionarily more conserved than would be expected on the basis of sequence conservation alone. The most reliable theoretical approach of developing 3D models is comparative modeling or homology modeling. The protein structures modeled by this technique has vast applications in structure-based drug discovery.

The basic principle behind comparative or homology modeling is based on the observation that the predicted protein structure will have similar structure with the protein with similar sequences.

The template structure used is experimentally developed structure, and the target structure is generated when it shares significant identity of more than 30% with the template. Various other structural genomic studies were initiated to elucidate new protein structures faster. The success of structural genomics is based on careful and optimal selection of proteins since experimental structure elucidation and comparative modeling complement each other [13].

Protein modeling requires expertise in structural biology and effective use of computer programming in each step of developing comparative model.

The process of homology modeling includes,[14]

- Identifying the known 3D structure-template
- Sequence alignment between target and template
- Building of 3D model using MODELLER9.19
- Validation/Evaluation/refining the model

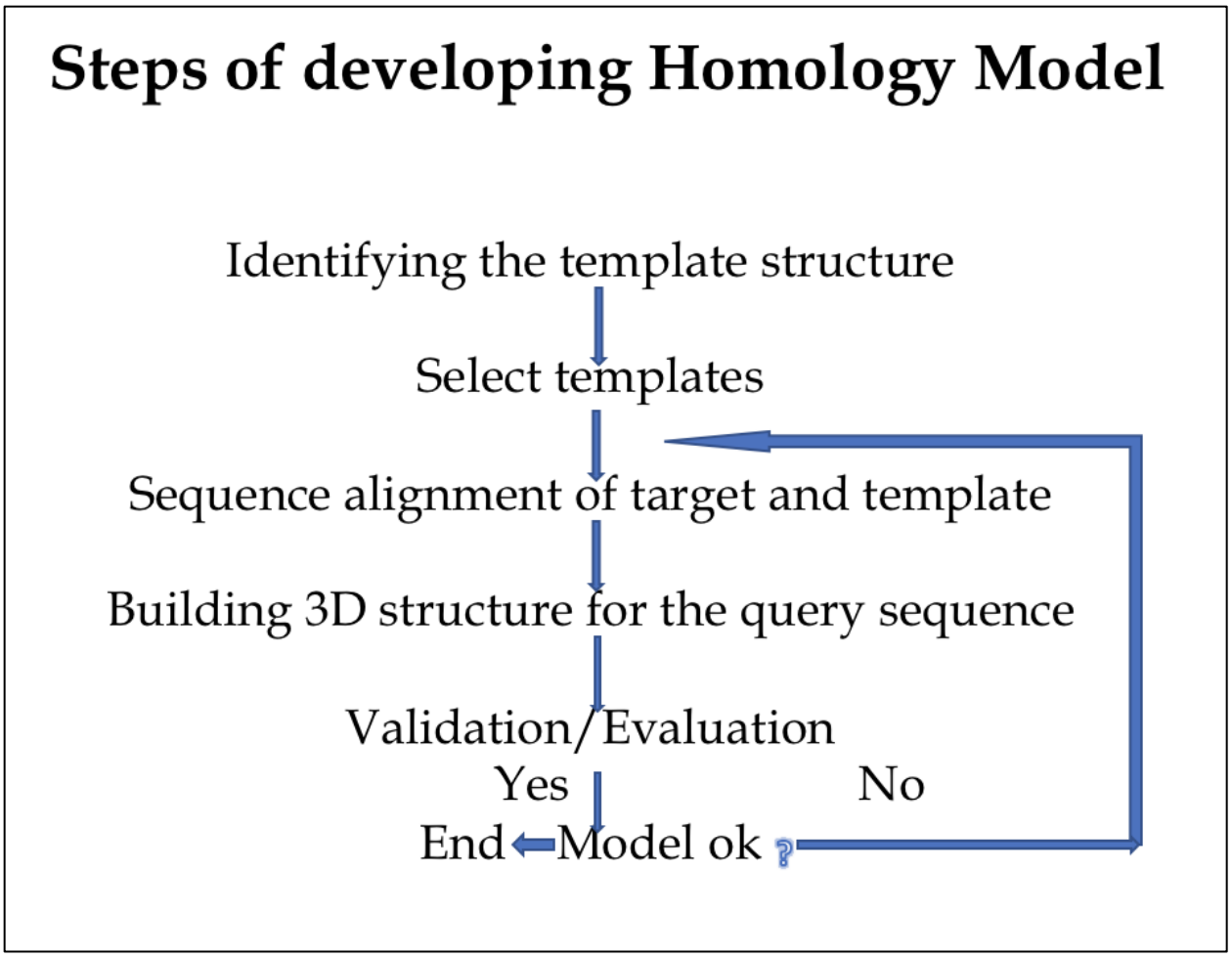

Figure 4. Basic steps involved in developing homology model.

a. Identifying the template and sequence alignment of target and template:

The principle of homology modeling is identification of one or more protein structures which likely resembles the structure of the query sequence. Later an alignment between the target and the template residues is produced. Protein structures are more conserved than protein sequences, if the sequence identity is less than 20% then building a structure is difficult. The percentage identity between the target and the template is determined by simple sequence alignment programs such as PDB BLAST or FASTA [15, 16].

b. Building of 3D model:

The alignment of target and template and the obtained template structure are used to build a model of the target. Protein structures are more conserved therefore the sequence similarity implies significant structural similarity.

c. Validation/evaluation/refining the model:

The developed homology model can be validated using QMEAN4, ProSA, Ramachandran plot, or docking to test the quality of the model [17],[18],[19]. The quality of the model depends on the quality of the sequence alignment and structure of the template. If there are alignment gaps present which are commonly called as indels, then building a model could be difficult, these indels are present in the target but are absent in template, this could lead to poor resolution to build the structure. As the sequence identity decreases the model quality declines, a model with ~1–2 Å root mean square deviation has 70% identity and model with 2–4 Å

agreement has 25% sequence identity. When the amino acid sequences of target and template proteins are completely different, errors are higher in the loop regions [20].

Models where some regions are constructed without the template using loop modeling, are considered less accurate than the other regions of the model. Identity of the model is also decreased when errors in side chain packing and position increase which leads to poor quality of the model. The presence of these various atomic position error can impede the use of models built through comparative modeling in study of protein-protein interactions, quaternary structure prediction and drug design [20].

High quality homology models of proteins can be obtained when the template and target are closely related, which has an important application in structural genomics, producing experimental structures for all protein folds of different classes. When the initial sequence alignment or template selection has errors it causes inaccuracies in homology modeling with low identity [21].

However, homology models can be used in formulating hypotheses about amino acids conservation, which leads to developing new experiments to test these hypotheses. For example, the spatial arrangement of the proteins, help to study interaction with a small molecule or another protein or nucleic acid [20].

d. MODELLER9.19:

MODELLER9.19 satisfies the spatial restrains of the proteins built by using comparative modelling. It is described as "Modeling by satisfaction of restraints". It uses restraints from protein structures which are developed using NMR and shares identity. We provide sequences to be

modelled along with the known structure. Modeler performs comparison of protein sequences and structures and calculates model with all non-hydrogen atoms[22].

7. Molecular Docking:

Molecular docking is a key tool for drug discovery. This approach can be used to study the interactions between a small molecule such as peptide and a protein at the atomic level, based on these docking interactions we can characterize the binding site of the target protein and study the fundamental biochemical processes [23]. Molecular docking involves two basic steps:

- Prediction of the ligand conformation in the active site of the protein.
- Ranking the conformations based on scoring function

Molecular docking uses sampling and scoring approach [24].

a. Sampling Algorithms:

With available degrees of translational, rotational and conformational freedom of both ligand and protein, huge number of binding modes can be generated between the molecules, which would be expensive to generate computationally, therefore various sampling algorithms such as Monte Carlo algorithm, matching algorithms etc., has been used in molecular docking software's.

b. Scoring Functions:

The principle of scoring functions is to generate correct orientations from incorrect orientations or binders from inactive compounds in a computational time frame. Scoring functions depends on estimating the binding affinity between the molecules rather than calculating, it adopts assumptions and simplifications.

Binding site prediction plays significant role in increasing the efficiency of docking, so predicting the site before docking gives effective docking models, if not the binding sites can be predicted using cavity detection methods like GRID, POCKET, PASS etc. Docking the molecule with protein without knowing the binding site is called Blind docking.

The principle of Molecular docking is based on Lock and Key theory by Fischer, where the ligand fits into the receptor like lock and key. During docking between Ligand and receptor, the interactions between the molecules leads to reshaping of the active site which suggests that both the molecules are flexible [25]. The different docking software's available are FlexX, AUTODOCK, HPEPDOCK, GOLD, etc.

8. The role of homology modeling and docking in experimental biology:

Molecular docking when combined with experimental data, analyzes drug metabolism. In order to determine the integrity of protein structure of Pituitary adenylate cyclase-activating peptide I receptor (PAC1R), Lusheng *et al*, studied the physicochemical properties of PAC1R by constructing a homology model. Later protein - ligand interactions were studied using molecular docking, they determined the interaction sites as Ile63, Ser100 and Gln105. Their analyses provided an evidence for development of PAC1R target drugs [26]. The potential of PLD2 in phospholipid industrial production was assessed by estimating the catalytic selectivity of PLD2 using homology modeling, docking and binding energy conformation.

9. Aims:

i. To study the role of LYCAT in cigarette smoke extract induced ROS and apoptosis in bronchial epithelial cells.

ii. To develop a homology model of LYCAT and to determine the active site using computer assisted tools.

iii. To study binding interactions between LYCAT homology model and peptide mimetic using molecular docking.

HYPOTHESIS: Based on the observation of increased LYCAT expression in lung epithelial cells by cigarette smoke extract (CSE), it is hypothesized that LYCAT regulates CSE mediated lung epithelial apoptosis via mitochondrial reactive oxygen species (ROS).

II. MATERIALS AND METHODS

1. Reagents:

Anti-GAPDH antibodies were purchased from Santa Cruz Biotechnology, Inc. (Santa Cruz, CA, USA). rabbit anti-LYCAT, anti-beta actin antibodies, Pen-Strep, fetal bovine serum (FBS), trypsin, Triton X-100, and Tween 20, were from Sigma-Aldrich, Inc. (St. Louis, MO, USA). Horseradish peroxidase (HRP)-linked anti-mouse IgG and anti-rabbit IgG antibodies were obtained from Bio-Rad Laboratories, Inc. (Hercules, CA, USA). FuGENE HD transfection reagent was obtained from Promega (Madison, WI). Phosphate-buffered saline (PBS) was obtained from Biofluids Inc. (Rockville, MD, USA). PARP, Caspase-3 from Cell Signaling (Danvers, MA, USA). FITC Annexin V Apoptosis Detection Kit was obtained from BD Biosciences (San Jose, CA, USA).

2. METHODS:

a. Cell culture:

Bronchial epithelial cell line Beas2B., an immortalized cell line transformed using an adenovirus 12-SV40 viral vector, was purchased from ATCC and were cultured in Dulbeco's Minimal Essential Medium (DMEM) complete medium (10% FBS, 1% Penicillin-streptomycin) at 37^0C and 5% CO2. These cells were allowed to grow to approximately 80-90% confluence.

b. Cigarette smoke extract (CSE):

CSE was purchased from [Research-grade cigarettes (3R4F)]; Kentucky Tobacco Research and Development Center at the University of Kentucky. Briefly, CSE was prepared by bubbling smoke from six cigarettes through 100 ml of FCS-free cell culture medium at a constant airflow. Smoked medium was then sterile filtered through a 0.20micrometer filter (Minisart; Satorius Stedim Biotech, Göttingen, Germany), split into aliquots, stored at ~20°C, and served as the 100% CSE stock solution with 40 mg/mL concentration. For treatment the cells were exposed to 40 μg/mL of Cigarette smoke extract in DMEM media, and the control cells received the equivalent volume of DMSO devoid of CSE suspended in DMEM media.

c. RNA isolation and Real time RT-PCR analysis:

For RT-PCR analyses, RNA was isolated from Beas2B cells cultured in 6-well plate using TriZOL reagent (Invitrogen Corp., Carlsbad, Calif) according to the manufacturer's protocol. RNA was quantified spectrophotometrically and 1μg of RNA was reverse transcribed using cDNA synthesis kit (Bio-Rad). iQ SYBR Green Supermix (Life Technologies) was used to perform real-time PCR using iCycler by Bio-Rad for amplification.

cDNA Reverse Transcription conditions:

	Step 1	Step 2	Step 3	Step 4
Temp (^{0}C)	25	37	85	4
Time (mins)	10	120	5	∞

Real Time PCR conditions:

95^{o}C for 10 mins followed by 40 cycles of 5 sec at 95°C, 30 secs at 60°C and 72^{o}C for 40 secs.

The primers used for amplification are given below:

GAPDH:

Forward primer: 5′-TGTGGGCATCAATGGATTTGG-3′

Reverse primer: 5′-ACACCATGTATTCCGGGTCAAT-3′

LYCAT:

Forward primer: 5′-TCAGAGAAGCACCTCCTCCA-3′

Reverse primer: 5′- CGTTTGTGGCACCAGAGTTG-3′

The housekeeping gene glyceraldehyde 3-phosphate dehydrogenase (GAPDH) served as an internal control and all samples were run in triplicates.

d.Western Blotting:

The cultured cells in 6 well plates were washed with ice cold PBS, after aspirating the medium, 125 µl of lysis buffer containing protease and phosphatase inhibitors was added to each well. Samples were homogenized with an electric homogenizer, sonicated, and centrifuged at 10,000×*g* at 4°C in a micro centrifuge for 10 minutes. The supernatants were collected in 1.5 mL tubes and the protein concentration determined using the BCA protein assay (Pierce Chemical, Rockford, IL). Cell lysates were boiled with 6X laemelli buffer for 5 minutes at 100^{0}C. Samples (30 µg) were then subjected to SDS-PAGE electrophoresis and transferred to nitrocellulose membranes (Bio-Rad, Hercules, CA) in transfer buffer Novex (Life Technologies, Grand Island, NY). Membranes were incubated for 1h at room temperature in blocking buffer (Tris-buffered saline with

0.05% Tween-20, TBST) supplemented with 1% bovine serum albumin and then incubated with the respective primary antibodies for LYCAT, PARP and Caspase 3 overnight at 4°C according to the manufacturer's instructions. After four 10-min washes with TBST, the membranes were incubated for 1h with the secondary antibody in TBST with 1% bovine serum albumin. The membranes were rinsed four times with TBST and the bands were detected using Supersignal luminol enhancer (Perbio Science UK Ltd., Cheshire, UK) followed by exposure to blue-light–sensitive film Hyperfilm (Amersham Biosciences UK Limited, Little Chalfont, UK). Equal protein loading was verified by re-probing of membranes with anti-β-actin antibody. The relative intensities of protein bands were quantified by densitometry using ImageJ software. Results were expressed as a ratio of specific protein signal to β- actin signal.

e. Total reactive oxygen species (ROS) generation:

CSE induced ROS generation in Beas2B cells was determined by the DCFDA fluorescence method. Beas2B were pre-incubated with CSE. Following exposure to CSE, cells were loaded with 10 μM DCFDA in DMEM basal medium and incubated at 37°C for 30 min, after which the medium containing DCFDA was aspirated and cells were washed twice with PBS at room temperature. The cells were examined under a Nikon Eclipse TE2000-S fluorescence microscope with Hamamatsu digital CCD camera using a ×20 objective lens and MetaVue software (Universal Imaging, West Chester, PA), and oxidized DCFDA fluorescence was quantified by Image analyzer.

f. Mitochondrial ROS generation:

Mitochondrial superoxide generation in Beas2B cells upon CSE challenge was determined by using MitoSOX TM red mitochondrial superoxide indicator. Briefly, the cells were loaded with 5μM MitoSOX TM reagent for fifteen minutes and washed twice in phenol-red free DMEM media. The cells were examined under Nikon Eclipse TE 2000-S fluorescence microscope and pictures were captured on a Hamamatsu digital charge-coupled device camera (Japan) using a 40X objective lens.

g. Determination of mitochondrial hydrogen peroxide:

Intracellular hydrogen peroxide levels were determined by a mammalian expression vector encoding a fluorescent hydrogen peroxide sensor pHyper (Evrogen, Moscow, Russia). Cells were grown on glass bottom 35-mm dishes, transfected with 1 μg/ml of pHyPer-mito plasmid using FuGene HD transfection reagent for 24-72 hours in serum free DMEM medium, and treated with Cigarette smoke extract as described. Cells were washed twice with Phenol Red free basal DMEM and fluorescence of pHyPer-mito in living cells was examined under a Nikon Eclipse TE 2000-S fluorescence microscope with a Hamamatsu digital CCD camera, using a ×60 objective lens. To calculate pHyPer-mito fluorescence intensity (pixels) similar rectangular cell periphery regions were selected in control and treated cells using MetaVue software (Universal Imaging Corp.). At least 6–10 cells were evaluated for each treatment in triplicate, averaged to three independent experiments, and background fluorescence from an empty dish was subtracted.

h. Determination of apoptosis by flow cytometry:

Bronchial epithelial cells were pretreated with Peptide control and peptide mimetic with 30 μM for 24 hours, followed by exposure to 40 μg/mL of Cigarette smoke extract or DMSO for 4 hours. The cigarette smoke extract induced apoptosis of Beas2B cells was assayed by flow cytometry. Flow cytometry was used to determine the apoptosis by staining the cells with Annexin V and Propidium iodide (PI). The cells were detached from the plate using cell striping solution. Briefly, cell pellet was stained in 1X binding buffer containing Annexin V for 15 minutes. Later the cells were stained with PI and subjected to flow cytometry analysis using Gallio's flow cytometry (Beckman Coulter).

i. Cardiolipin analysis

i.i Extraction of cardiolipin from Bronchial epithelial cells and separation by thin layer chromatography:

Beas2B cells were treated with 40 μg/mL of CSE, and protein estimation was determined by BCA assay. Cell lysates were extracted using Bligh and Dyer method (Bligh EG, and Dyer WJ. A rapid method of total lipid extraction and purification. Can J Biochem Physiol. 1959;37(8):911-917), with chloroform/methanol (2:1 v/v). The cell lysate along with the organic solvents were vortexed, followed by addition of 1.0 mL of $CHCl_3$ and 1.0 mL of 0.1M KCl, vortexed and centrifuged at 3000 rpm for 5', the lower $CHCl_3$ layer was removed and dried under N_2, later the volume was made to 1.0 mL with $CHCL_3$. Cardiolipin was separated on the silica gel 60 plates coated with Magnesium acetated (7.5%) using the solvent system consisting of

chloroform/methanol/concentrated ammonia/water (65/25/4/1 v/v/v/v) in first direction and chloroform/acetone/methanol/acetic acid/water (30/40/10/7/5 v/v/v/v/v) in the second direction. Lipids were visualized on TLC plates by placing them in Iodine chamber. The separated lipids were scraped from TLC plates and analyzed for total lipid phosphorus using Fiske-Subbarao's method.

i.ii Determination of fatty acid composition of Cardiolipin:

The lipid extracts from Beas2B cells before and after treatment with CSE were subjected to alkaline methanolysis at 90°C for 120 min and the fatty acid methyl esters were analyzed by gas chromatography-mass spectrometry (GC-MS) method with C17:0 (heptadecanoic acid) as the internal standard (16-18). Fatty acid methyl esters were analyzed by gas chromatography-mass spectrometry (GC-MS, Shimadzu Scientific Instruments, Columbia, MD) equipped with Restek column (18). Levels of fatty acids and cardiolipin were expressed as mole% and nmoles/mg protein. The unsaturated to saturated fatty acid ratio (USR) was calculated by dividing the total amount (e.g. mole%) of the unsaturated fatty acids by the total amount (e.g. mole%) of the saturated fatty acids. The unsaturation index (USI) for each unsaturated fatty acid within cardiolipin was calculated by multiplying the number of double bonds in each fatty acid by the mole% of that fatty acid and dividing by 100. The USI for each phospholipid was calculated by adding the individual unsaturated fatty acid USI.

j.Measurement of LYCAT activity:

LYCAT activity was determined where the reaction mixture contained 50 mm Tris/HCl (pH 7.0), 25 μM 16- NBD-16:0 CoA, and Beas2B cell lysate (200 μg protein) in a total volume of 200 μl. The reaction mixture was incubated at room temperature for 30 min, following which the lipids were extracted, dried under nitrogen stream, and separated by thin layer chromatography (TLC) with chloroform:methanol:water (65:25:4, v/v/v). Fluorescent-labeled cardiolipin and monolysocardiolipin, separated on the TLC plates, were analyzed by GE ImageQuant LAS4000 analyzer and quantified by Image J. The specific activity of LYCAT was calculated and normalized with the enzyme in control lung tissue. The data were expressed as mean ± SEM.

l. Statistical Significance:

All data are expressed as means ± SEMs from at least three independent experiments, and results were subjected to statistical analysis by using a two-tailed Student *t*-test. Values of $P < 0.05$ were considered significant and were indicated with "*".

***In-silico* Analysis**

a. Homology Modeling:

Databases/Software's	**URL**
NCBI	https://www.ncbi.nlm.nih.gov/pubmed/
BLAST	https://blast.ncbi.nlm.nih.gov/Blast.cgi
PDB	https://www.rcsb.org/
SWISSMODEL	https://swissmodel.expasy.org/
MODELLER9.19	https://salilab.org/modeller/9.19/release.html
CASTp	http://sts.bioe.uic.edu/castp/index.html?2011
RASMOL	http://www.openrasmol.org/
HPEPDOCK	https://omictools.com/hpepdock-tool

Table 1. Software's and Websites used for developing 3D model of LYCAT and studying binding interactions between peptide mimetic and Homology model.

b. Sequence of the LYCAT protein and template identification:

The LYCAT protein had a molecular weight of 44.39 KDa and 376 amino acids which was already deposited at NCBI. A sequence similarity search was performed using protein BLAST tool to identify templates for homology modeling. To find structurally similar protein with the query, a sequence similarity was performed by running NCBI protein BLAST against Protein Data

Bank. The template was identified based on maximum score, smaller e value and >30% identity. 1BD2 protein was selected based on the identity which was greater than 46%.

c. Model building of the query using MODELLER 9.19

MODELLER9.19 was used along with an automated approach to comparative modeling by satisfaction of spatial restrains to develop models. After manually modifying the alignment input file in MODELLER9.19 to match template and query sequence, five models were build and they were thermodynamically minimized using molecular dynamics and simulation approach. By using MODELLER9.19 auto-model class, we can calculate three dimensional models of the target automatically. The Lowest Objective Function is used to select the best model by the smallest value of normalized Discrete Optimized Molecule Energy (DOPE) score. These models were then checked in detail for protein structure stereochemistry using Ramachandran plot, ProSA and Molecular Docking[22].

d. **DOPE: discrete optimize protein energy:**

DOPE is used to assess homology models, and the quality of a structure model. DOPE is an atomic -distance dependent statistical potential calculated from a sample of native protein structures. It is calculated based on probability theory[27].

e. **Ramachandran Plot:**

Ramachandran plot is used to visualize dihedral angle phi and psi of amino-acids residues in protein structure[19]. These two torsion angles of the polypeptide chain, also called as Ramachandran angles, describes the rotations between N-Cα (called Phi, φ) and Cα-C (called Psi, ψ). This plot provides viewing the distribution of torsion angles, and an overview of allowed and disallowed regions of torsion angle, which is an important factor for quality assessment of three-dimensional protein structures. Ramachandran plot can be obtained using SWISSMODEL quality assessment or PROCHECK[28].

f. ProSA:

Protein Structural Analysis helps to recognize the errors in the experimental and theoretical models of proteins structures, it validates the protein structure. The overall quality score of the input structure is determined, based on the score errors in the native protein. The Z-score plot of the input file is obtained, which contains the z-scores of all experimentally determined protein chains and compares the Z-score of predicted model whether it's in the range of native proteins. It also provides 3D structure with residues energies, red indicates increasing energy while blue indicates low energy[18].

g. QMEAN4:

It is a composite scoring function, which derives the function value for both global (entire structure) and local (per residue) from a single model. By default this QMEAN4 value is converted to z-scores, to relate with existing high resolution X-ray and NMR structures[17].

h. HPEPDOCK:

HPEPDOCK is a hierarchical flexible-peptide docking protocol. It integrates with several other programs such as FASTA, MODELLER., etc. The initial step in docking is to provide the input files, in PDB file formats for both protein and peptide. Homology model of LYCAT structure developed by MODELLER9.19 is used for docking and the peptide mimetic sequence is converted to a structure to perform HPEPDOCK. With the input files which were provided the peptide is docked against whole LYCAT homology model. Since the binding site is not being provided, HPEPDOCK docks the peptide to possible binding positions on the receptor LYCAT. Based on binding orientations and energy scores docking models are available[29].

i. CASTp:

Computed atlas and surface tomography of proteins is used to locate, delineate and measure the concave surface regions on 3D structure of proteins. It identifies voids in the interior of the protein and pockets located on the protein surfaces. These measurements are calculated analytically. CASTp is primarily used to study surface features and functional regions of the proteins [30].

III. RESULTS

1. *In vitro* analysis

1.a Expression of LYCAT protein in human lung tissues from non-smokers and smokers.

Lung tissue lysates (~20 μgs protein) (n=9) from non-smokers and smokers were subjected to SDS-PAGE and probed for LYCAT expression by Western blotting with anti-LYCAT antibody. It was found that the LYCAT protein expression was accentuated in the smoker's lung homogenates compared to that of Non-smokers as seen in Figure 1A, 1B. Based on the results, we conclude that LYCAT expression is enhanced by cigarette smoking.

1.b Expression of protein and mRNA levels of LYCAT in Bronchial epithelial cells exposed to cigarette smoke extract.

To further investigate the protein expression of LYCAT in lung epithelium, Beas2B bronchial epithelial cells were challenged with 40 μg/mL of Cigarette smoke extract for 2 hours. CSE exposure increased LYCAT protein expression in Beas2B cells (Figure 6A, 6B) and the LYCAT protein expression was quantified by densitometry and normalized to β Actin.

Real time PCR was performed to detect the expression of LYCAT mRNA induced by CSE. Beas 2B cells seeded on 6 well plates were grown to 80-90% confluence and treated with 40μg/mL of CSE at different time points (30 min,1h and 2h) and total RNA was isolated using TRIZOL reagent from cigarette smoke extract treated and control epithelial cells. 1μg of RNA was reverse transcribed using cDNA synthesis kit. For real-time RT PCR, SYBR Premix Ex Taq (Takar) was

used and the amplification reactions were performed in triplicate. LYCAT mRNA expression was quantified with respect to GAPDH. Exposure of Beas2B cells CSE increased LYCAT mRNA levels at each of the time point (Figure 6C). Based on the results, we conclude that LYCAT protein and mRNA expressions are enhanced in lung epithelial cells exposed to CSE.

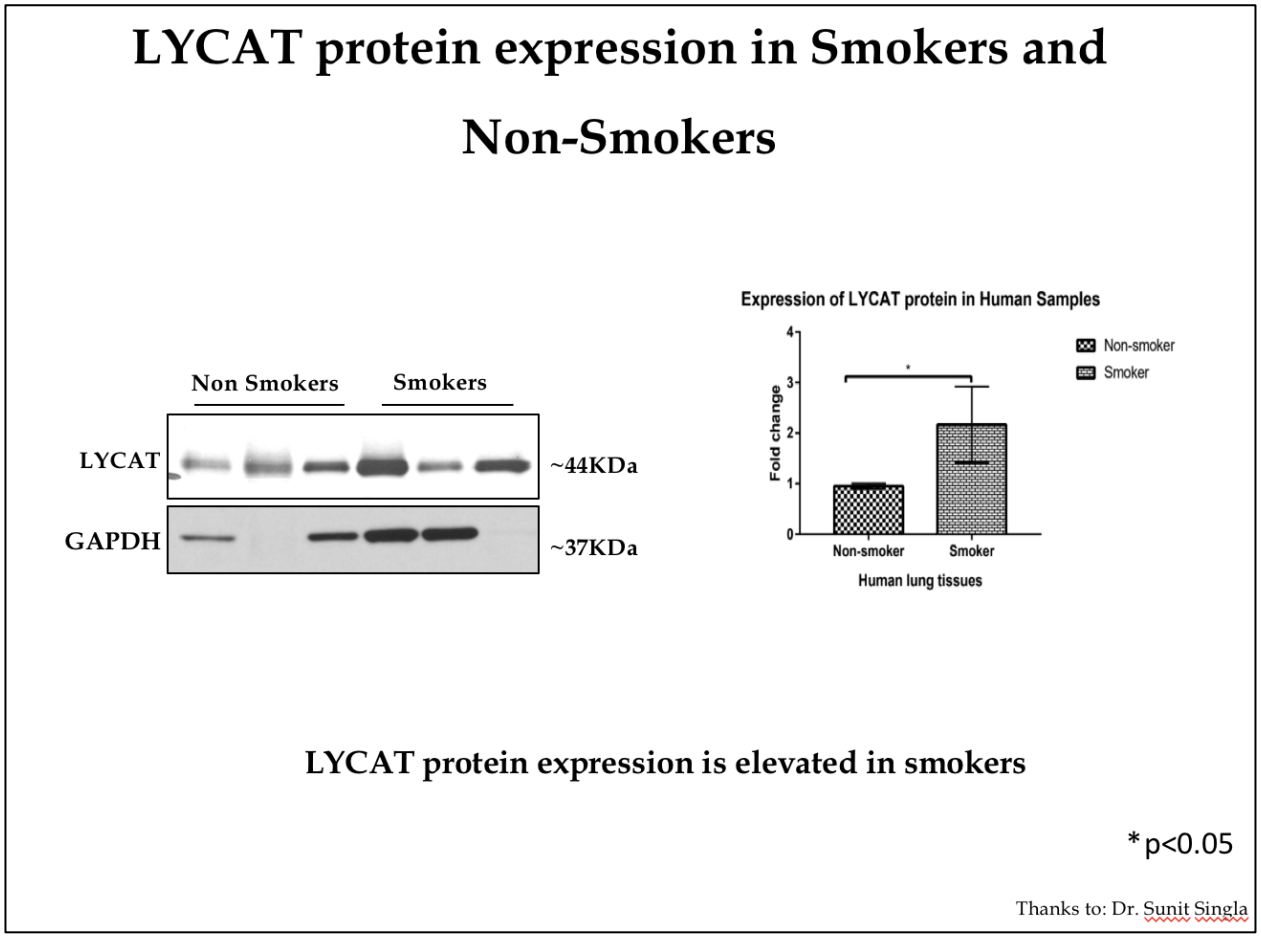

Figure 5. LYCAT protein expression in Human lung tissues from non-smokers and smokers and Beas2B cells exposed to CSE for 2 h**. A.** Representative western blot, **B.** quantification of the expression of LYCAT.

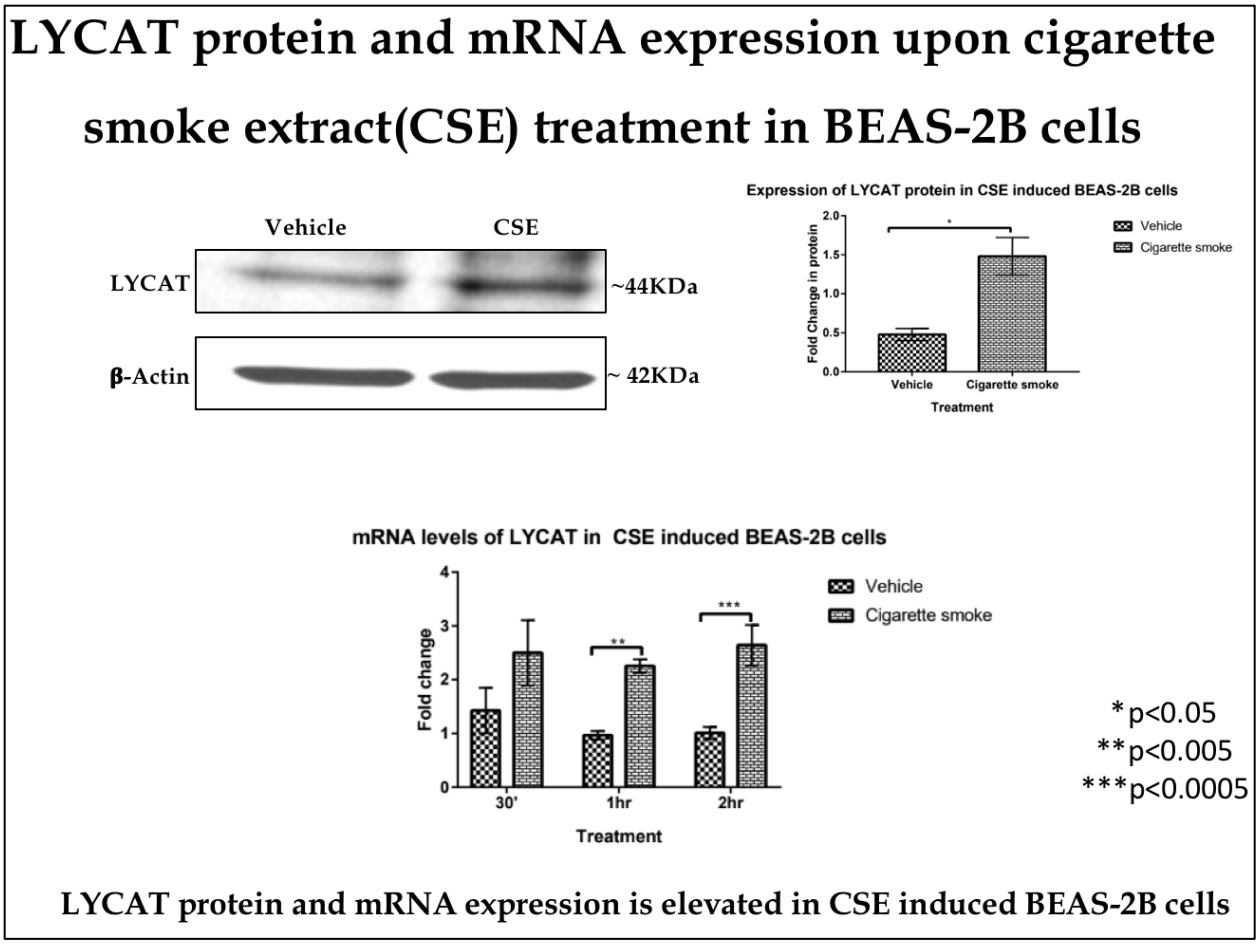

Figure 6. Expression of LYCAT protein and mRNA Beas2B cells exposed to CSE. **A.** Representative western blot for expression of LYCAT in CSE induced Beas2B cells. **B.** Quantification of the expression of LYCAT protein. **C.** Representative quantification of the mRNA levels of LYCAT protein.

1.c Cigarette smoke extract enhances total ROS in Bronchial epithelial cells:

Cigarette smoke extract induced total ROS in cells was detected using 2',7'-dichlorodihydrofluorescein diacetate (DCFDA) method. Beas 2B cells seeded in 35-mm dishes were grown to ~ 70% confluence and treated with CSE (40 μg/well) for 15', 30', 1h and 2h. After the treatment, cells were assayed for total ROS production using DCFDA. Cells were incubated with 10 μM of DCFDA reagent for 30 min, media was aspirated, and cells were examined under Nikon 40X objective lens. Statistical analyses performed for the fields which were randomly chosen, using Image J. As shown in Figure 7, CSE stimulated total ROS production in Beas2B cells as determined by DCFDA oxidation at 15',30', 1h and 2 h post-CSE challenge.

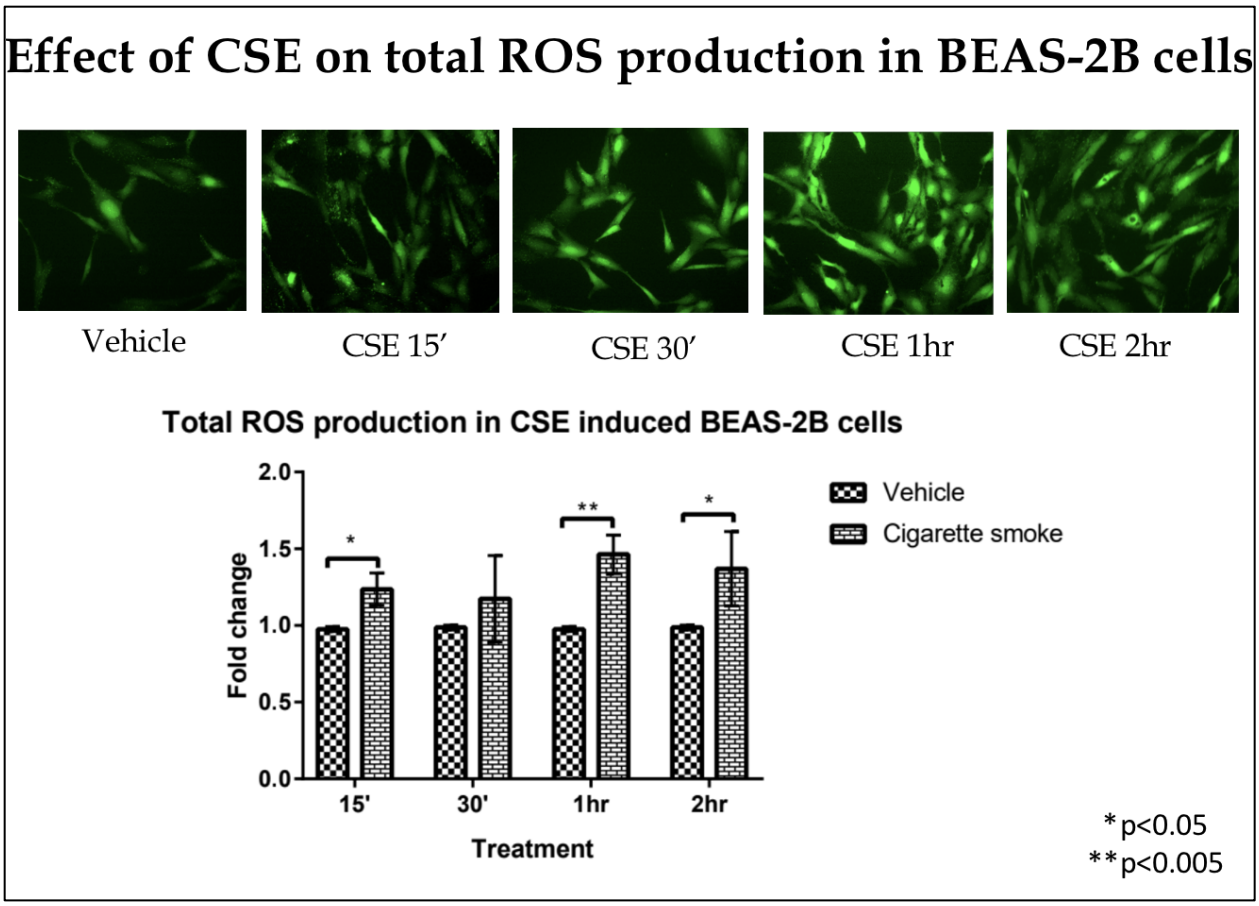

Figure 7. Total ROS production in CSE induced Beas2B cells. **A**, is a representative Total ROS production images, **B**. is a representative quantification of the ROS production in CSE induced Beas2B cells.

1.d Blocking LYCAT with a peptide mimetic attenuated cigarette smoke extract induced total ROS:

Cigarette smoke induced total ROS formation in cells was detected and quantified by fluorescence microscopy. Beas2B cells seeded in 35-mm dishes were grown to ~70% confluence and treated with control peptide or LYCAT peptide mimetic (30 μM) for 24 h. After pre-treatment, the cells were incubated with DCFDA for 30 mins and treated with CSE (40 μg) for 1h and was assayed for total ROS production using DCFDA method. The cells were examined under Nikon 40X objective lens. Statistical analysis is performed to the fields which were randomly chosen, using Image J. The LYCAT peptide mimetic attenuated CSE induced total ROS production in Beas2B cells compared to control peptide (Figure 8).

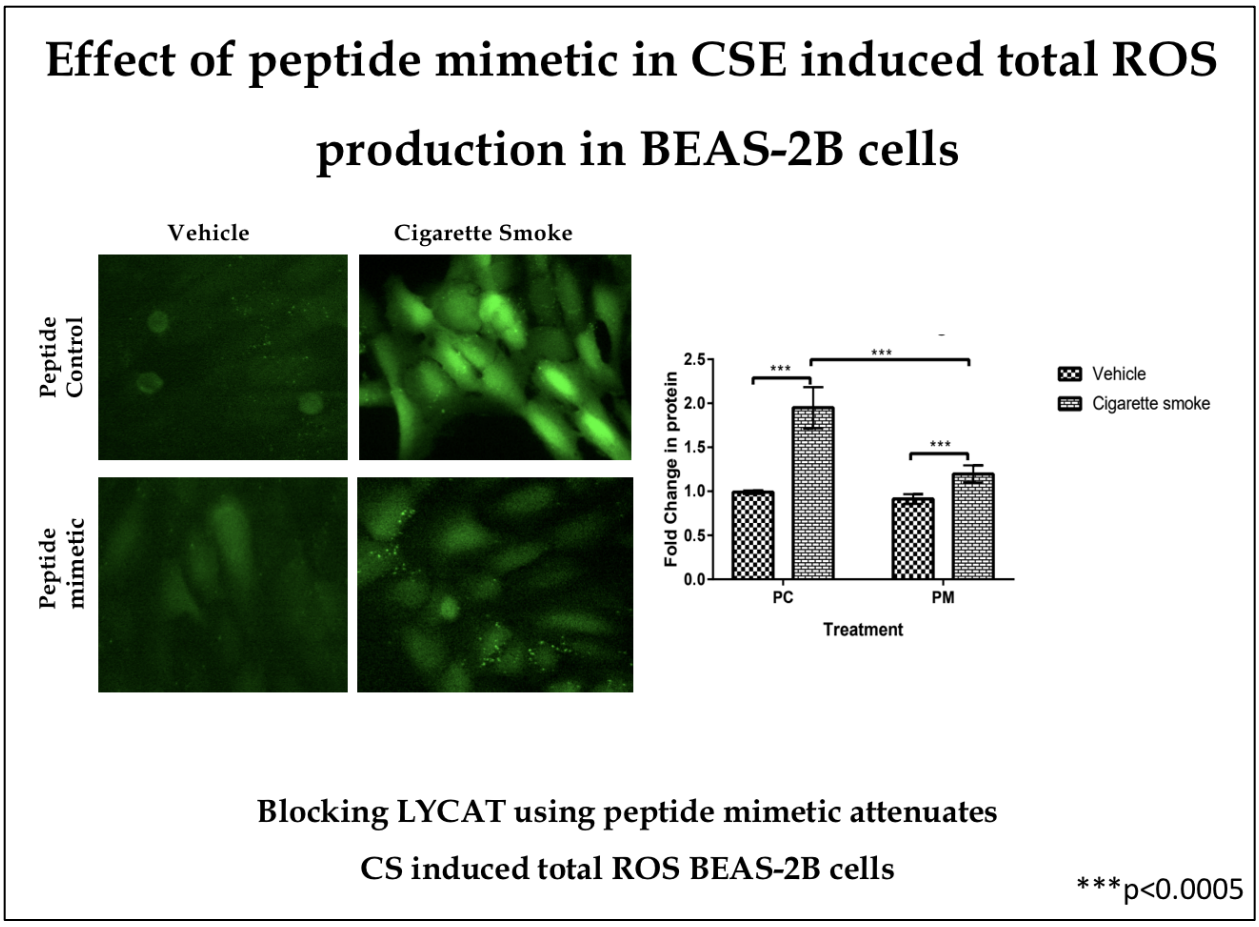

Figure 8. Inhibition of LYCAT by peptide mimetic attenuates CSE induced total ROS. **A**. is a representative image of total ROS production and **B.** representative quantification of the attenuated Total ROS production by peptide mimetic.

1.e Cigarette smoke extract induces mitochondrial ROS in bronchial epithelial cells:

CSE - induced mitochondrial ROS in Beas2B cells was detected using MitoSOX. Beas 2B cells seeded in 35-mm dishes were grown to ~ 70% confluence and treated with CSE (40 μg/well) for 15', 30', 1h and 2h. After the treatment, cells were assayed for mito-ROS production using MitoSOX (5 μM) for 15', media was aspirated, and cells were washed with phenol red free media twice and examined under Nikon 40X objective lens. Statistical analysis is performed for the fields which were randomly chosen, using Image J. As shown in Figure 9, CSE stimulated mito ROS production in Beas2B cells at all time points post-CSE challenge.

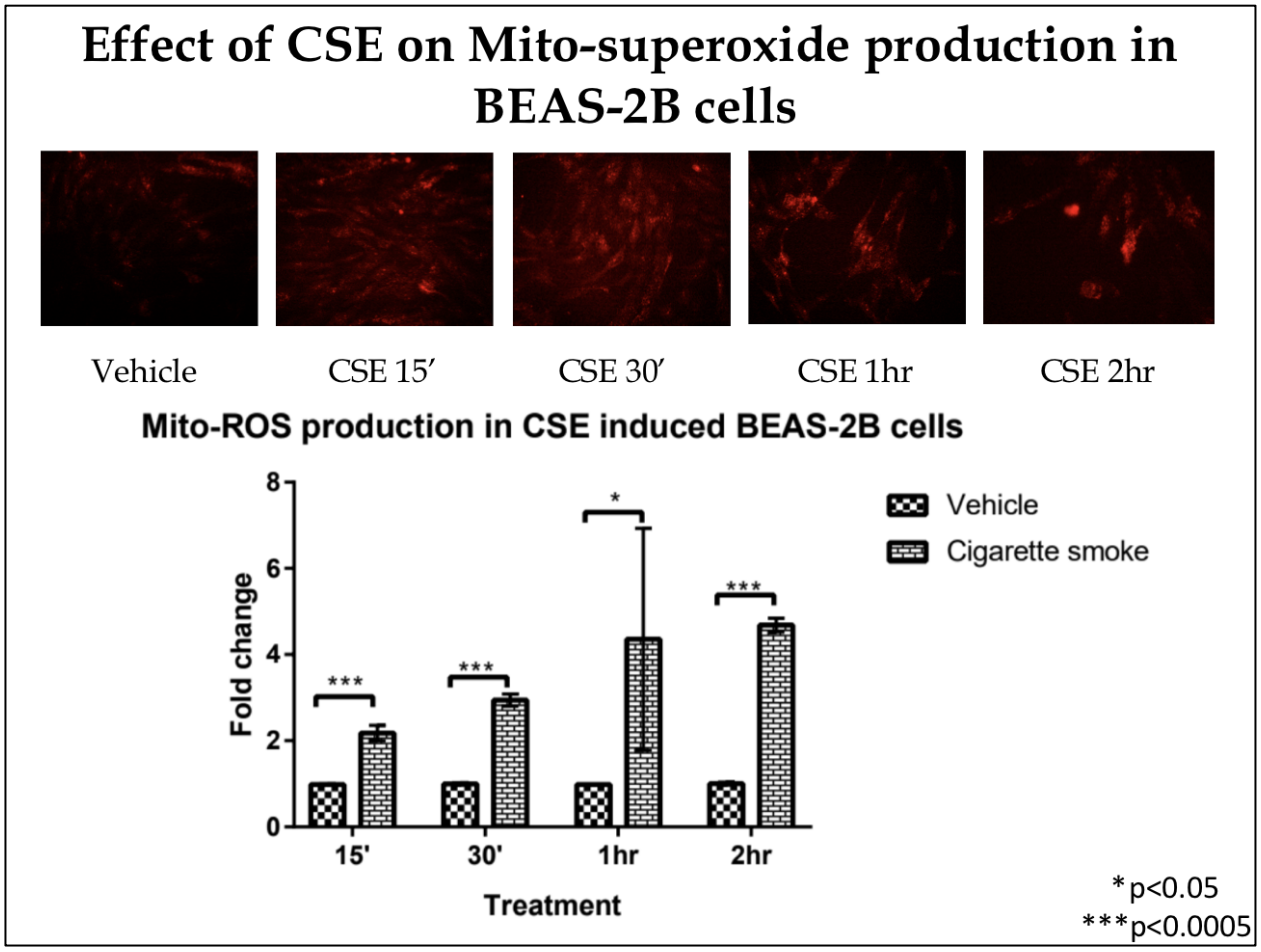

Figure 9. Mito-ROS production in CSE induced Beas2B cells. **A**, is a representative Mito ROS production images, **B**. is a representative quantification of the Mito ROS production in CSE induced Beas2B cells.

1.f Blocking LYCAT with peptide mimetic attenuates CSE- induced mitochondrial superoxide:

Having demonstrated that CSE stimulated LYCAT expression and mito- superoxide in Beas2B cells, we next investigated the role of LYCAT in CSE-mediated mito- superoxide Beas2B cells, grown to ~80% confluence, were pre-treated with control or LYCAT peptide mimetic (30 μM) for 24 h prior to exposure to CSE (40 μg/ml) for 2 h. Mito-ROS was assayed by using MitoSOX as outlined above. As shown in Figure 10, cells pre-treated with LYCAT peptide mimetic showed reduced mito- superoxide production compared to cells treated with CSE without LYCAT peptide mimetic.

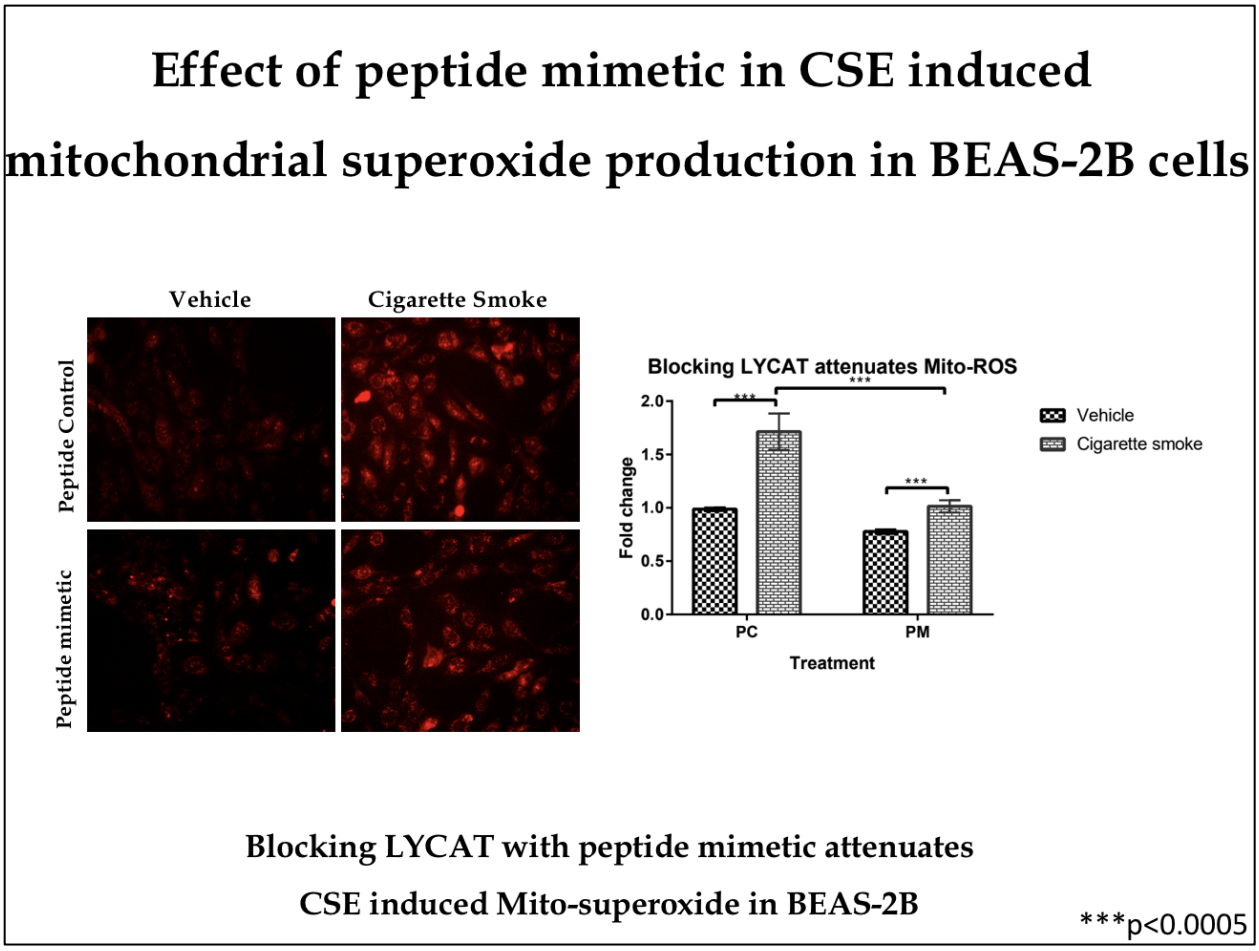

Figure 10. Inhibition of LYCAT by peptide mimetic, attenuates CSE induced mito superoxide. **A**. is a representative image of mito superoxide production and **B.** representative quantification of the attenuated mito superoxide production by peptide mimetic.

1.g LYCAT peptide mimetic attenuates CSE-induced mitochondrial-Hydrogen peroxide using p-Hyper plasmid:

In addition to MitoSOX, we also used a specific mitochondrial targeted plasmid to measure mito-ROS production. Beas2B cells were transfected with GFP-tagged empty vector or RFP-tagged p-Hyper plasmid (1 μg/ml) for 48 h, and cells were viewed under immunofluorescence for the expression of RFP tag, and ~40% of cells were transfected with the p-Hyper plasmid. After 48h, cells were pre-treated with LYCAT peptide mimetic (30 μM) for 24 h prior to CSE challenge for 2 h. Cells were viewed under the microscope for the oxidation of the insert to green fluorescence by generation of hydrogen peroxide. As shown in Figure 11, the LYCAT peptide mimetic effectively attenuated CSE-induced mito-Hydrogen peroxide production.

These results complemented the data from MitoSOX experiments.

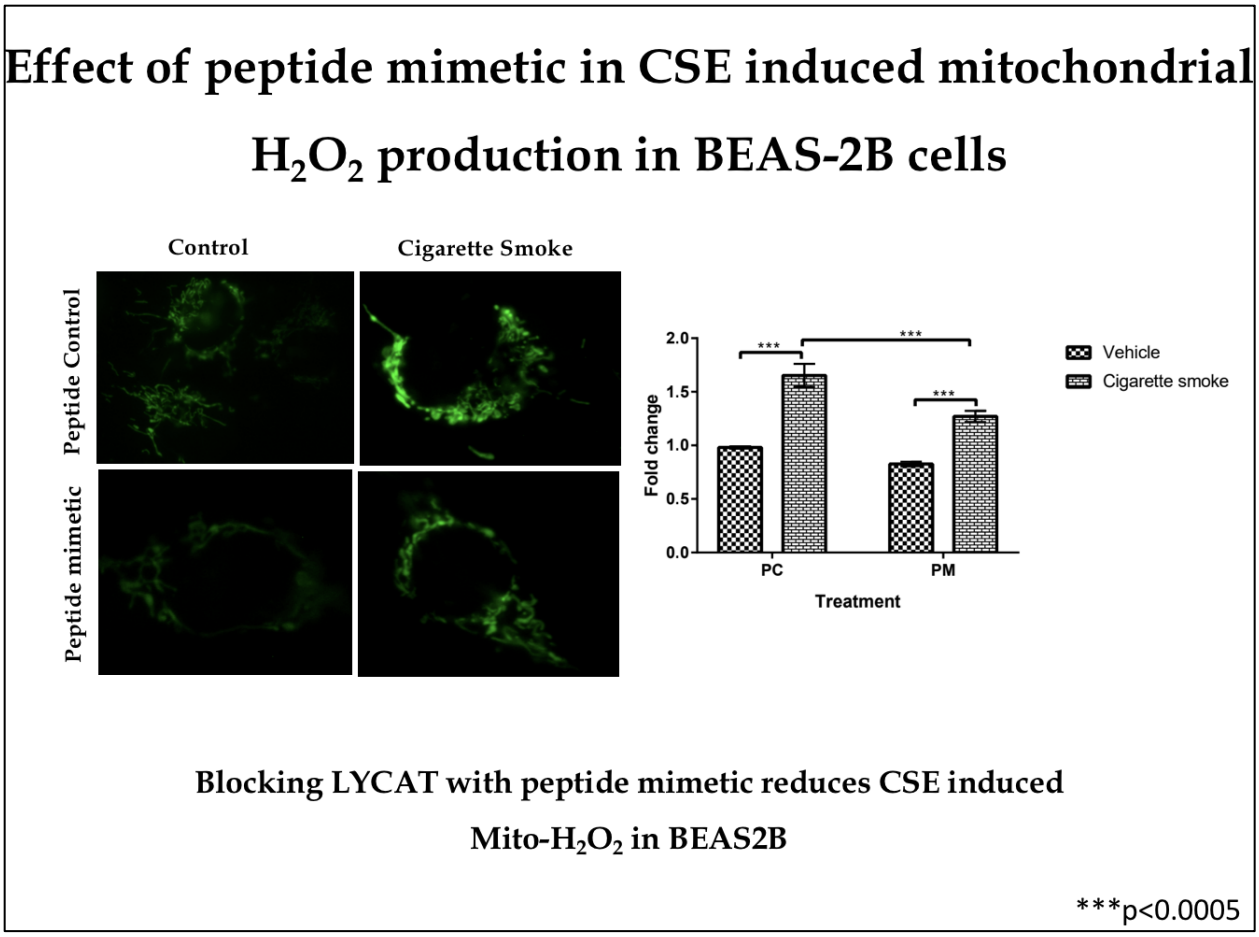

Figure 11. Inhibition of LYCAT by peptide mimetic, attenuates CSE induced mitochondrial super-oxide. **A**. is a representative image of superoxide production and **B.** representative quantification of the attenuated superoxide production by peptide mimetic.

1.h Cigarette smoke extract up-regulates apoptosis in Beas2B cells and blocking LYCAT with peptide mimetic ameliorates CSE-mediated apoptosis

Next, the role of LYCAT in CSE-induced apoptosis of Beas2B cells was investigated using the LYCAT peptide mimetic. Beas2B cells were grown to ~70% confluence and pre-treated with LYCAT peptide mimetic (30 μM) for 24 hours. Cells were then treated with CSE (40 μg/ml) for 4 h and apoptosis was determined by Western blotting or flow cytometry. Treatment of Beas2B cells with CSE induced cleavage of Caspase 3, a marker of apoptosis. To study the role of LYCAT in CSE-mediated apoptosis, LYCAT activity was blocked with a peptide mimetic. Beas2B cells were pre-treated with peptide control/peptide mimetic (30 μM) for 24 h followed by CSE exposure (40 μg/ml) for 4 h. The control and cigarette smoke treated cells were analyzed for apoptosis by flow cytometry. The % of apoptotic cells analyzed by flow cytometry was reduced by LYCAT mimetic suggesting a role for LYCAT in CSE-induced apoptosis (Figure 12).

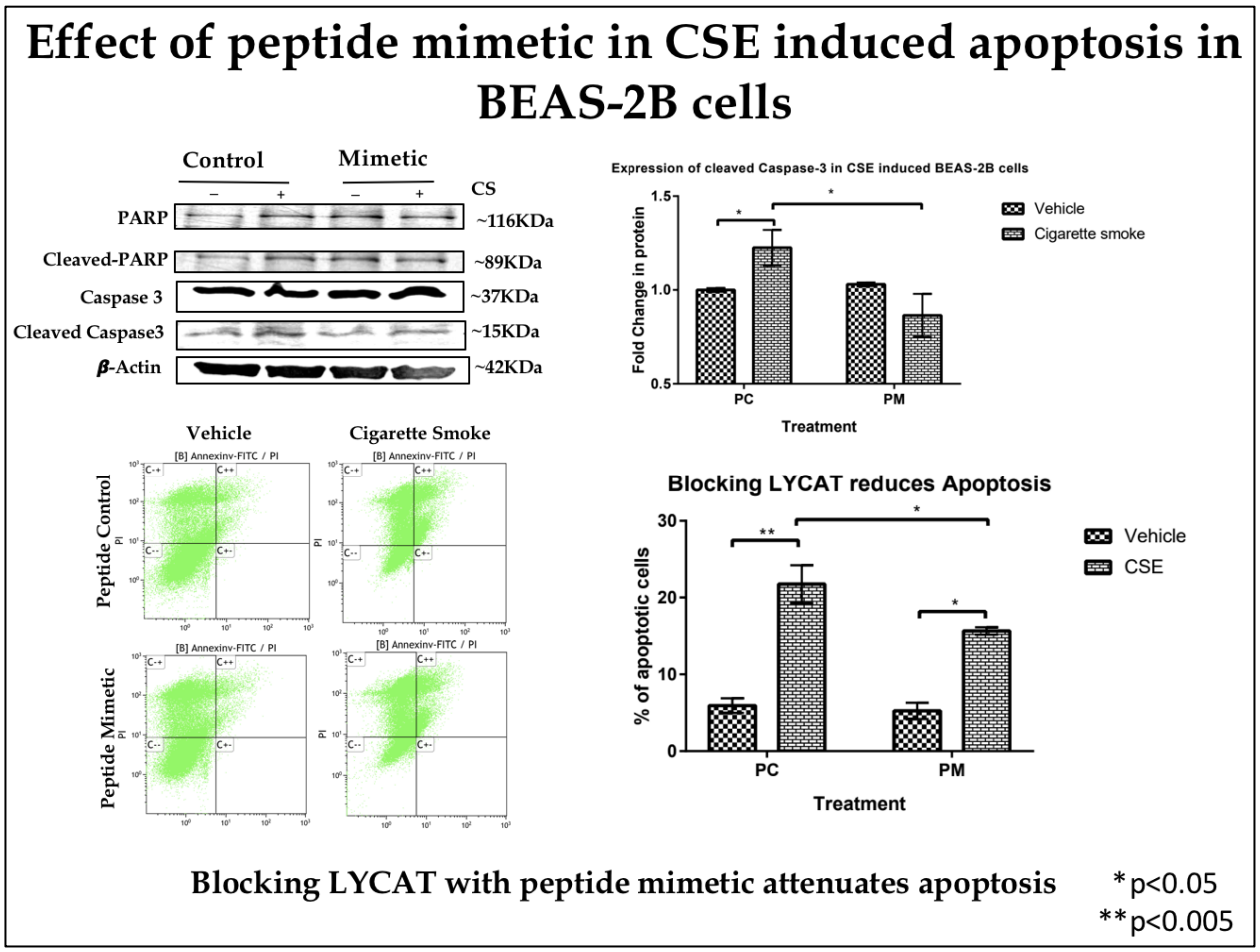

Figure 12. The effect of LYCAT peptide mimetic on CSE induced expression of cleaved caspase-3. **A**. representative western blot for cleaved caspase 3 expression, **B.** quantification of the expression of Cleaved caspase 3. Flow cytometry analysis of % of apoptotic cells in CSE induced Beas2B cells and LYCAT inhibited Beas2B cells, **C.** representative plots for late apoptotic cells in CSE induced Beas2B cells, **D**, quantification of the late apoptotic cells.

1.i Separation of phospholipids by Thin Layer Chromatography (TLC) and determination of cardiolipin levels:

Beas 2B cells were seeded on 100mm dishes and treated with 40Ug/mL of Cigarette smoke extract, cell lysates were subjected to lipid extraction using 2:1 chloroform: methanol, and were later suspended in chloroform, 120 nmol of lipid was loaded on TLC plates and subjected to 2-dimensional TLC plates containing 7.5% Magnesium Acetate (20 cm X 20 cm plate). The plate was developed in the first dimension with: $CHCl_3$:CH_3OH: NH_4OH:H_20 (62:25:3:1 (v/v/v/v)) in the first direction, dried in the hood for 20 min and run in the second direction with the solvent system: $CHCl_3$: Acetone:CH_3OH: Acetic Acid: Water (30:40:10:7:5 (v/v/v/v/v)). After development in the second direction, the plates were air dried, and lipids were visualized under I_2 vapors, marked and lipid phosphorus quantified. The experiment was performed as duplicates, where A, B are controls and C, D are cigarette smoke treated lipid extracts. In the figure, ABCD, different lipids were separated. After separation the TLC plates were scraped and total lipid phosphorus was estimated and we observed no significant change in lipid phosphorus between control and treated (Figure 13).

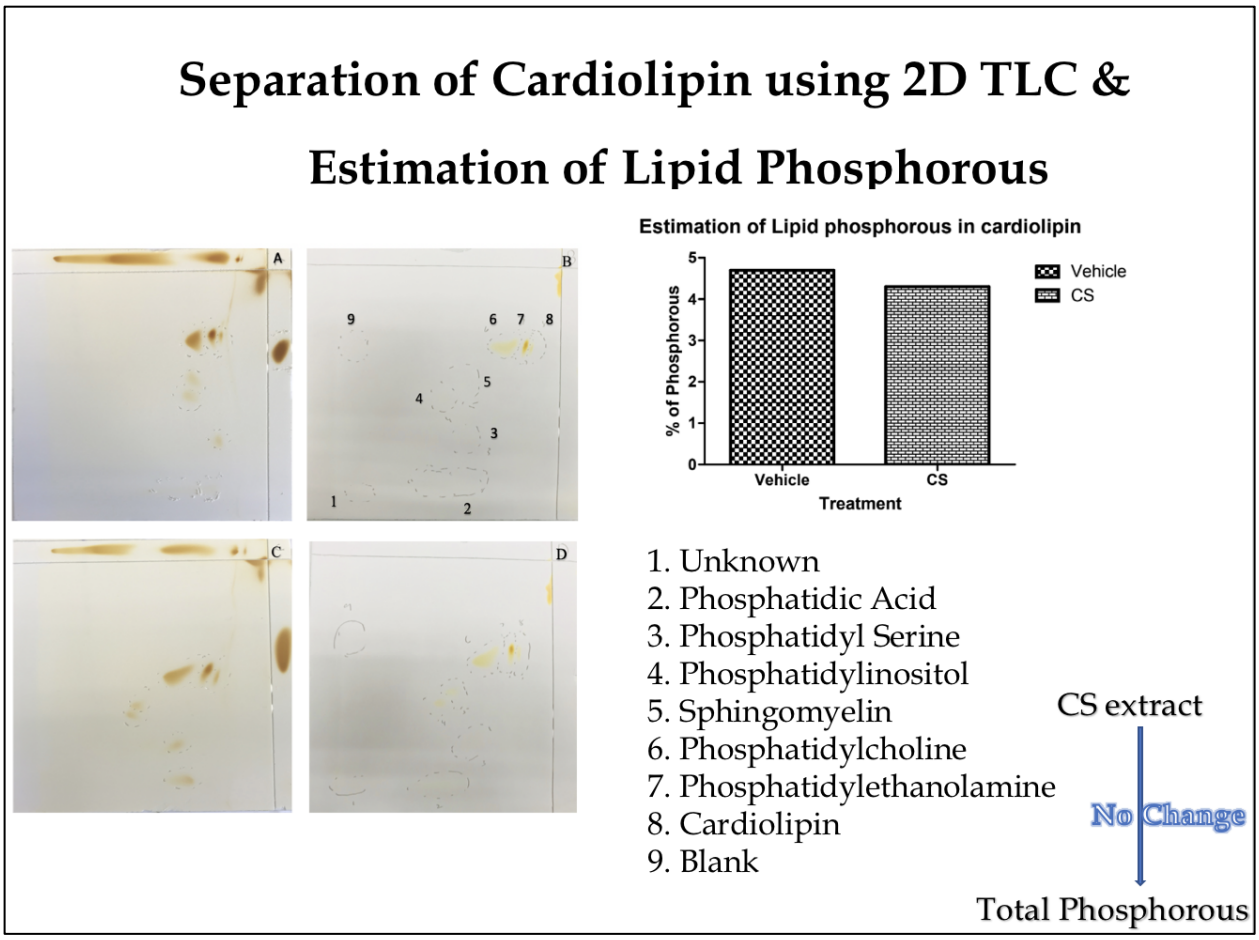

Figure 13. Separation of Phospholipids using 2D dimensional Thin Layer Chromatography and Estimation of Lipid Phosphorus in Control and CS extracts., **A.** representative images of the separated phospholipids by 2D TLC, **B.** quantification the total lipid phosphorus in lipid phosphorus.

Table 2. Estimation of total Phosphorus for Control-A

Number	Lipids	Absorbance of A	Absorbance of B	% of P For A	% of P For B
1	-	0.212	0.072	2.60946486	0.11
2	PA	0.252	0.088	7.35179083	1.77666667
3	PS	0.325	0.078	16.0065357	0.79666667
4	PI	0.22	0.087	3.55793006	1.63
5	SM	0.237	0.088	5.57341859	1.77666667
6	PL	0.527	0.307	39.9552819	23.2016667
7	PE	0.36	0.174	20.1560709	10.1116667
8	**CL**	**0.27**	**0.112**	**4.74291876**	**4.0325**
9	BL	0.19	0.068	0.00118558	0.00

Table 3. Estimation of total Phosphorus for CSE-C

Number	Lipids	Absorbance of C	Absorbance of D	% of P For C	% of P For D
1	-	0.114	0.071	-0.0006463	0.01166667
2	PA	0.166	0.224	8.00070781	15.1125
3	PS	0.15	0.081	5.53875271	1.04166667
4	PI	0.14	0.090	4.00003077	1.92416667
5	SM	0.16	0.090	7.07747465	1.875
6	PL	0.41	0.354	45.5455231	27.7616667
7	PE	0.28	0.222	25.5421379	14.8675
8	**CL**	**0.17**	**0.130**	**4.30809829**	**5.7975**
9	BL	0.114	0.066	-0.0006463	0

1.j GC-MS:

The extracted Lipids from control and cigarette smoke extract were subjected to GC/MS and this study concluded that there was change in fatty acid composition, in CSE compared to control. A, B are controls and C, D are CSE treated samples.

Percentage of Fatty acid:

	A	**B**	**C**	**D**
15:00	0.13	0.13	0.07	0.01
17:00	0.01	0.02	0.02	0.08
18:1 (n-9)	56.29	55.62	65.09	67.30

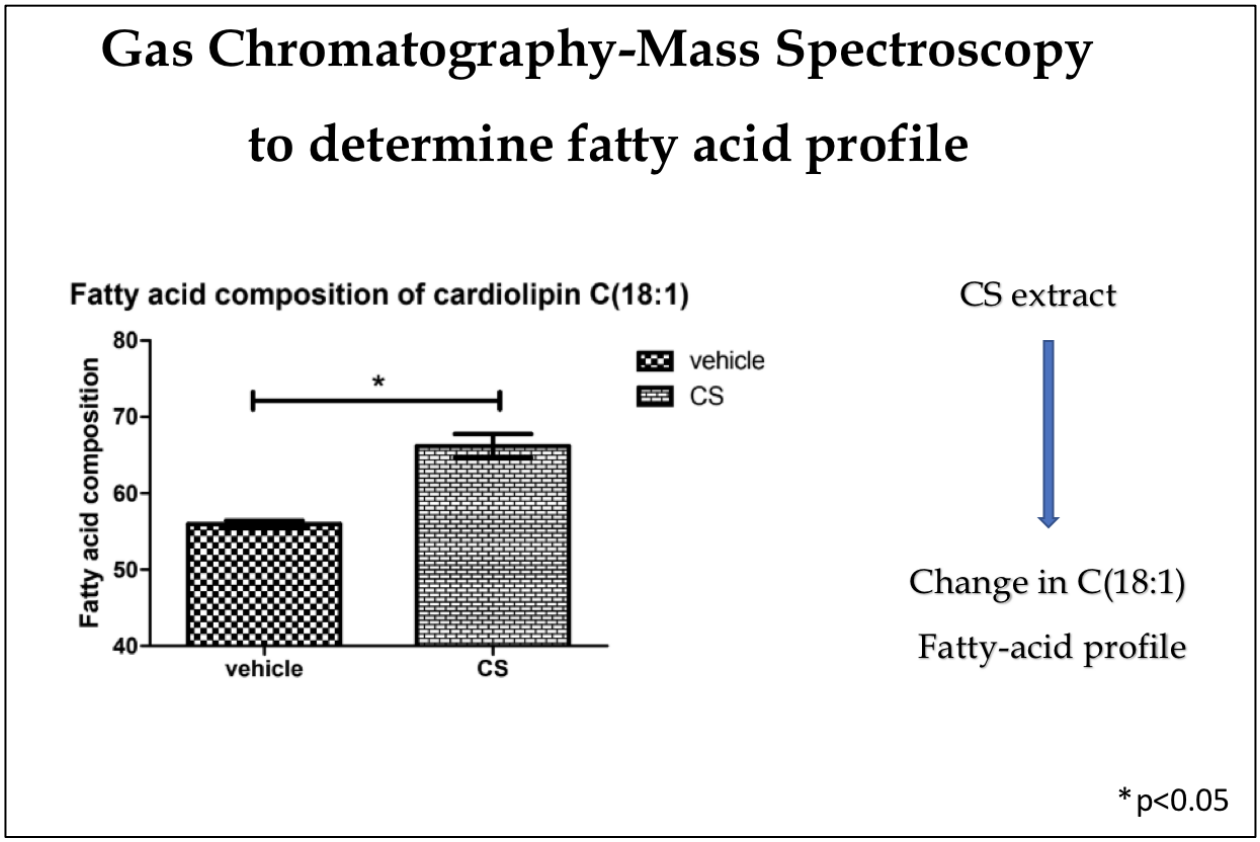

Figure 14. Estimation of Fatty acid composition in control and CSE lipid extract and a representative quantification of the fatty acid composition of C (18:1).

1.k. LYCAT mimetic attenuates LYCAT activity in Beas2B LYCAT over expressed cells

The efficacy of LYCAT peptide mimetic to inhibit LYCAT activity was tested in Beas2B cells overexpressing LYCAT WT adeno vector (25 MPI, 24 h). As shown in Figure 15, cells treated with LYCAT peptide mimetic (30 μM) for 1h effectively inhibited LYCAT activity.

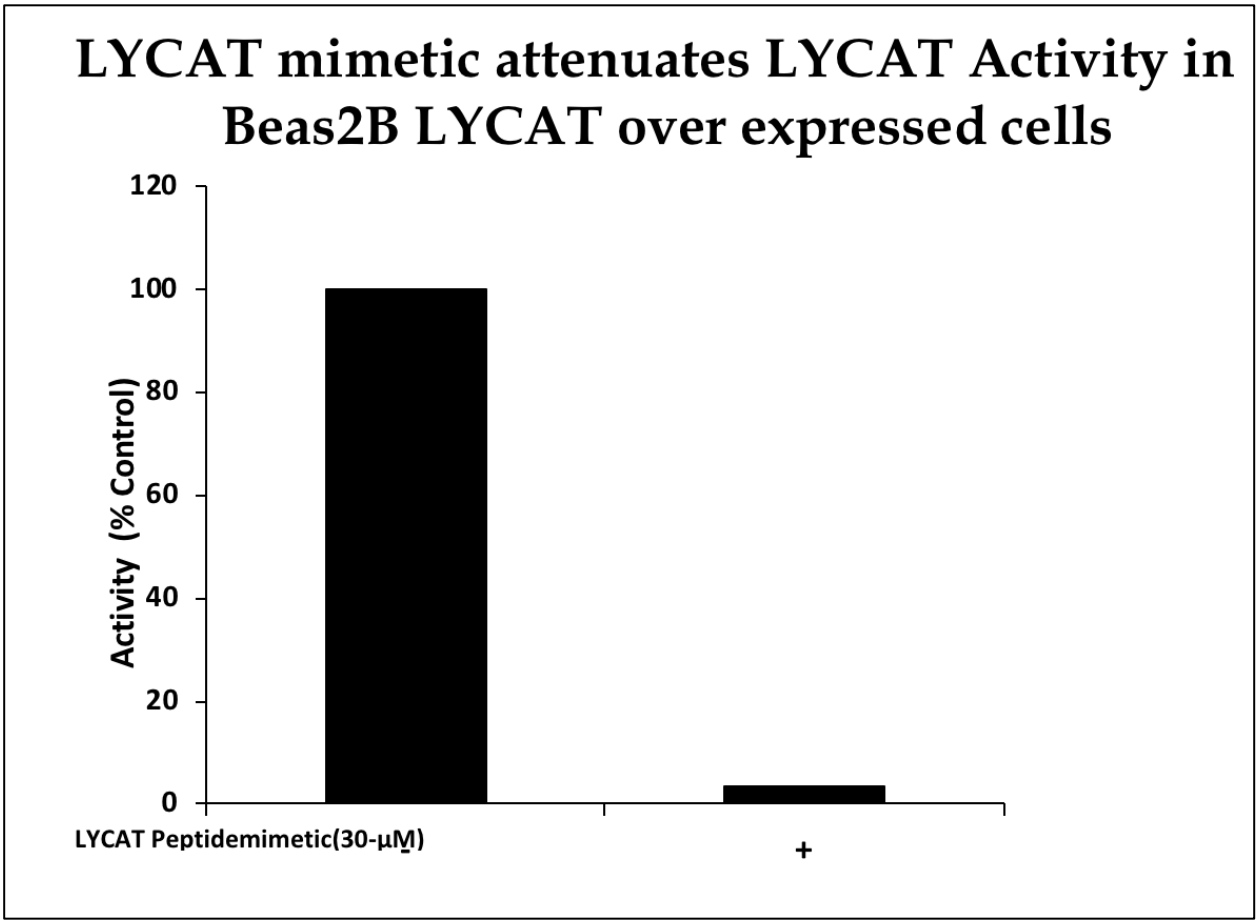

Figure 15. Effect of peptide mimetic on LYCAT activity in LYCAT overexpressed Beas2B cells, where the activity of the LYCAT overexpressed Beas2B cells was attenuated, the above quantification is representative plot for attenuation LYCAT activity.

2. *In-silico* Analysis

Homology Modelling of LYCAT protein:

a. LYCAT protein structure evaluation:

In protein data bank (PDB), the 3D structure of the LYCAT protein was not reported, therefore a 3D model of LYCAT was developed using comparative modeling techniques. The basic principle of homology modeling is building an unknown structure of the protein based on known structure and sequence similarity. The amino acid sequences for LYCAT was retrieved from NCBI, and subjected to BLAST against the Protein Data Bank, to determine a suitable template structure for modelling. Protein with PDB ID 1BD2, was selected based on the low "e" values and sequence similarity. The chain length of LYCAT protein is 376 amino acid residues. Based on the identity >46% between the query and template, 1BD2 was selected.

FASTA

lysocardiolipin acyltransferase 1 isoform 2 [Homo sapiens]

NCBI Reference Sequence: NP_001291374.1

GenPept Identical Proteins Graphics

```
>NP_001291374.1 lysocardiolipin acyltransferase 1 isoform 2 [Homo sapiens]
MVSWKGIYFILTLFWGSFFGSIFMLSPFLPLMFVNPSWYRWINNRLVATWLTLPVALLETMFGVKVIITG
DAFVPGERSVIIMNHRTRMDWMFLWNCLMRYSYLRLEKICLKASLKGVPGFGWAMQAAAYIFIHRKWKDD
KSHFEDMIDYFCDIHEPLQLLIFPEGTDLTENSKSRSNAFAEKNGLQKYEYVLHPRTTGFTFVVDRLREG
KNLDAVHDITVAYPHNIPQSEKHLLQGDFPREIHFHVHRYPIDTLPTSKEDLQLWCHKRWEEKEERLRSF
YQGEKNFYFTGQSVIPPCKSELRVLVVKLLSILYWTLFSPAMCLLIYLYSLVKWYFIITIVIFVLQERIF
GGLEIIELACYRLLHKQPHLNSKKNE
```

Figure 16. The FASTA sequence of the LYCAT retrieved from NCBI database.

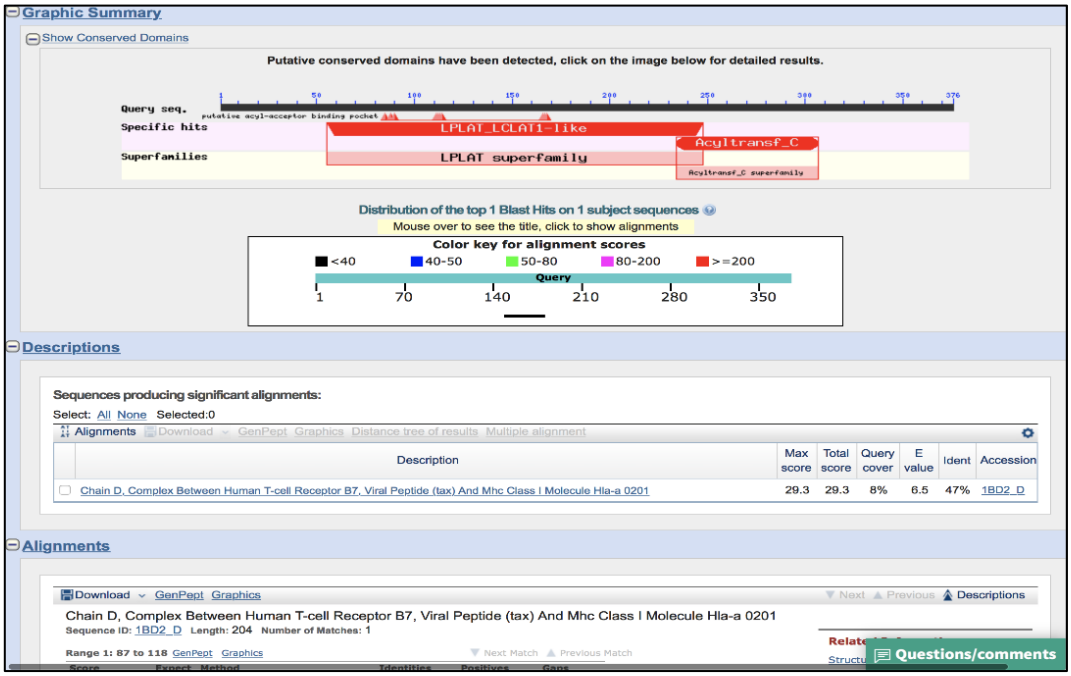

Figure 17. Similarity search of query sequence (LYCAT) using PDB-BLAST

Figure 18. Structure of template protein 1BD2 obtained from PDB-BLAST

b. MODELLER9.19:

Using MODELLER9.19 program, the 3D structure of the target LYCAT protein was obtained. Among the five models generated by MODELLER9.19, the model with Lowest objective function was considered to be the best model for further structure validation. The figure xx shows the prominent secondary arrangements of the developed three-dimensional model of the LYCAT protein

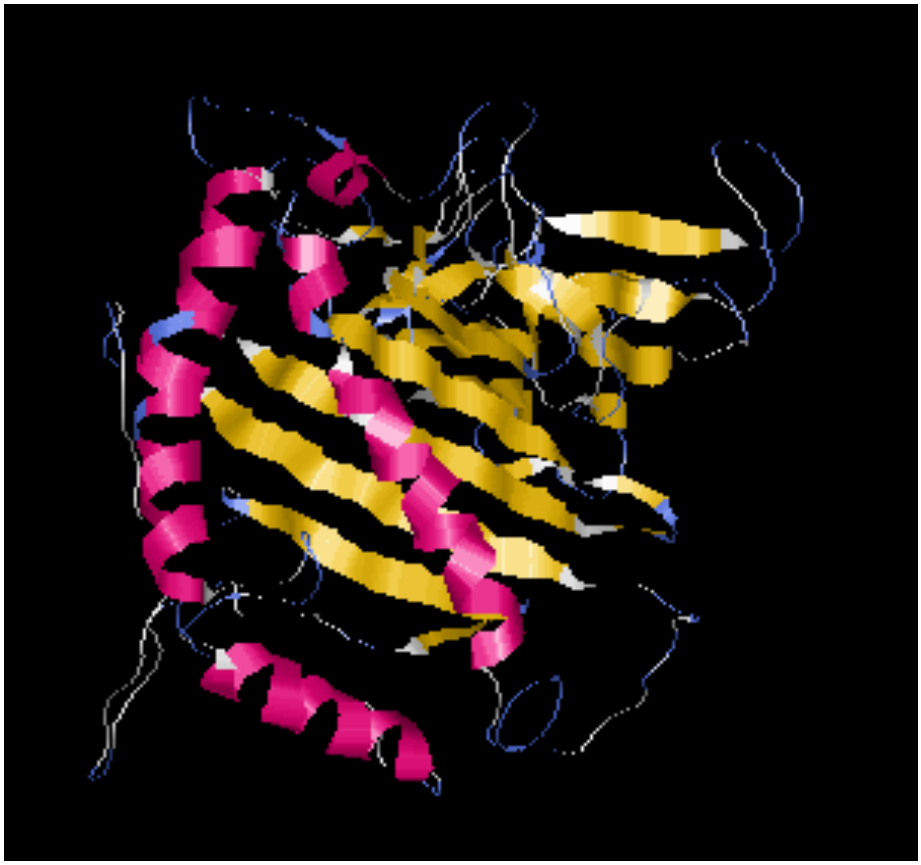

Figure 19. Homology model of LYCAT viewed by using RasMol. The LYCAT homology model represented as cartoon where helices were represented in pink, sheets in yellow and loops in blue.

c. Validation of LYCAT protein structure:

The developed 3D model of LYCAT protein was validated for the stereochemical quality using SWISSMODEL structural analysis. Predicted .pdb format of the LYCAT protein was analyzed for the estimation of the quality of the model.

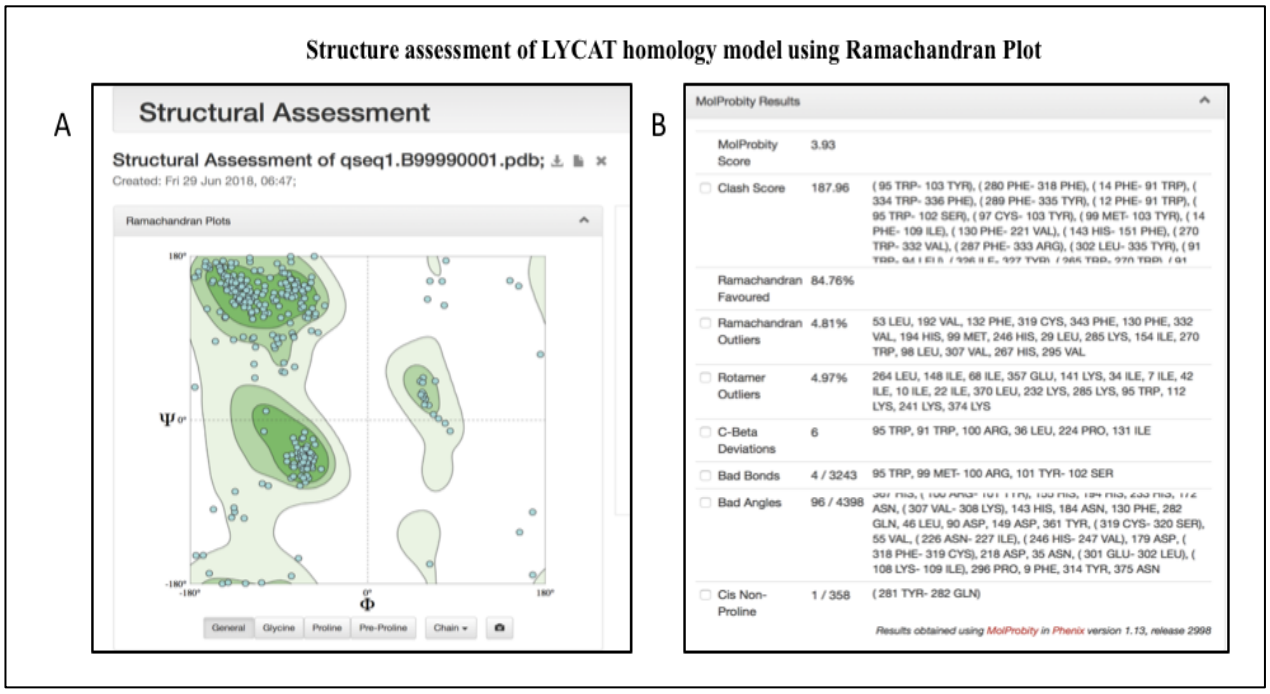

Figure 20. The figure displays the Ramachandran plot for LYCAT protein showed that 84.76% residues were in the favored region (green), 4.81% were in allowed region (light green) among 376 amino acid residues. This model is of better quality and further refinement can be done to achieve 90% of favored region.

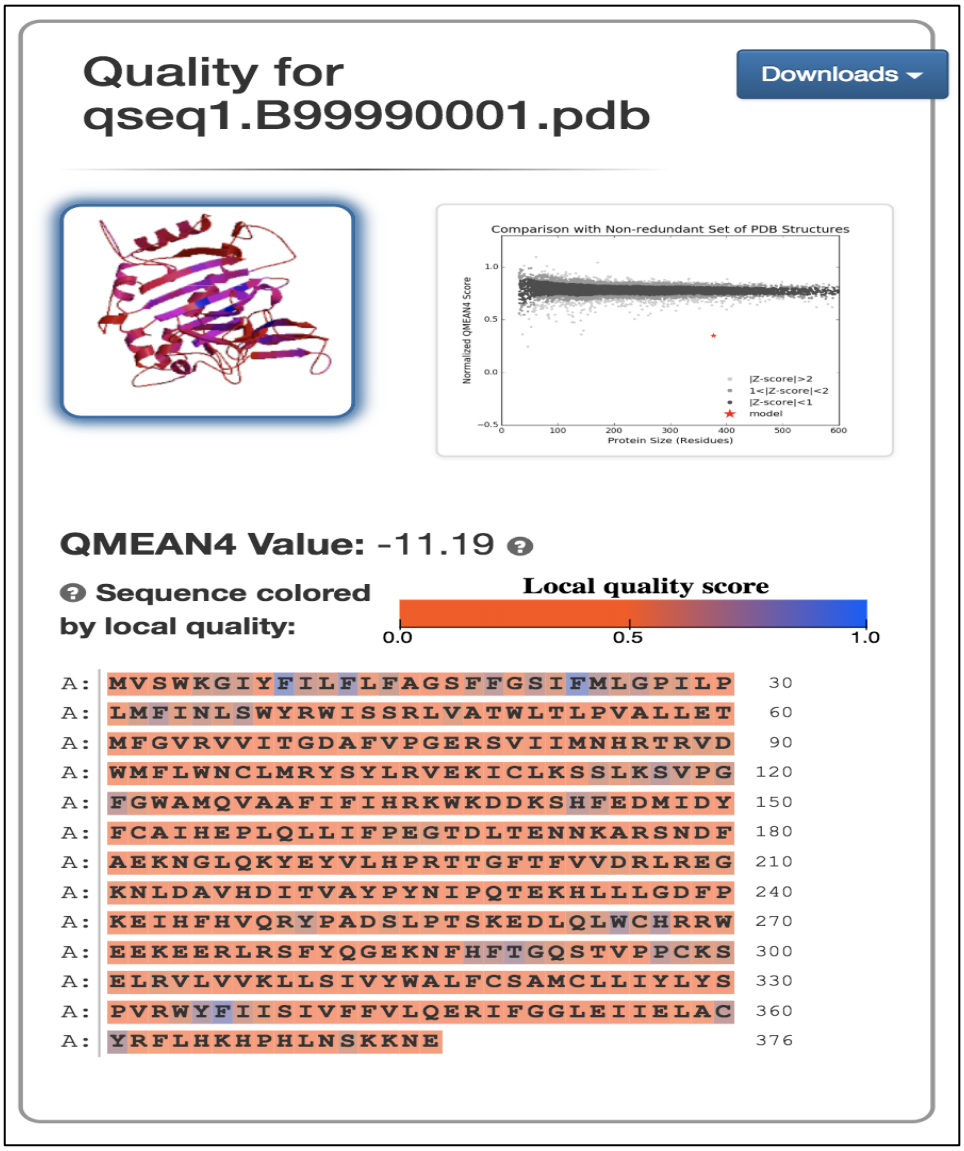

Figure 21. The QMEAN4 score was -11.19, the Z score was -0.94 predicted by SWISSMODEL structural assessment.

A B

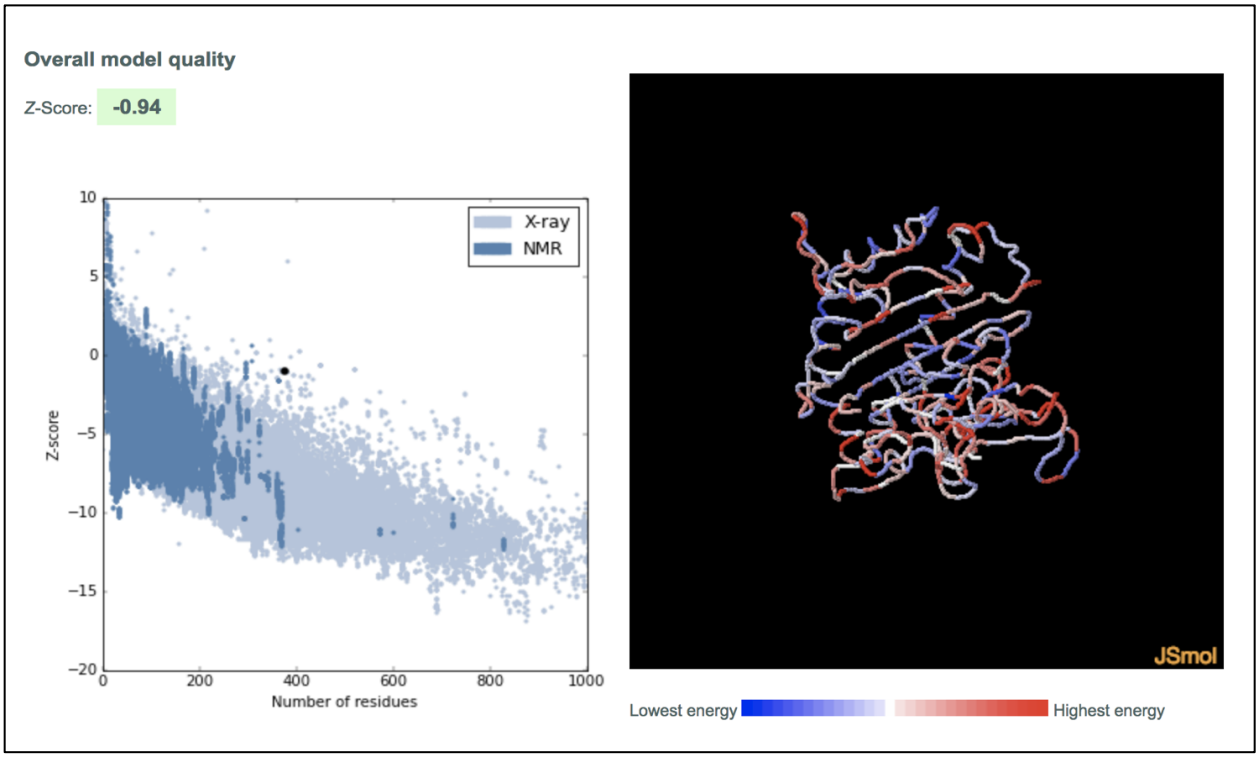

Figure 22. The Z score of the LYCAT protein is -0.94 which is represented as a large dot in the Figure 22A, the energies depicting the amino acids of the 3D model are shown in the Figure 22B. These values were predicted by ProSA, where the Z scores of the chains of proteins in PDB is determined by NMR (dark blue) and X-ray crystallography (light blue).

d. Prediction of active site by CASTp:

The biological active site of the LYCAT protein was predicted using CASTp server. Here the surface topography of the 3D LYCAT was predicted and the surface area and volume of all the expected pockets and cavities on the 3D structure of the enzyme was measured. The surface area and volume of the largest pocket was 1417.854 $Å^3$ and 2029.864 $Å^2$ respectively. This largest pocket is considered to be the biologically active site of the LYCAT enzyme (Figure 23).

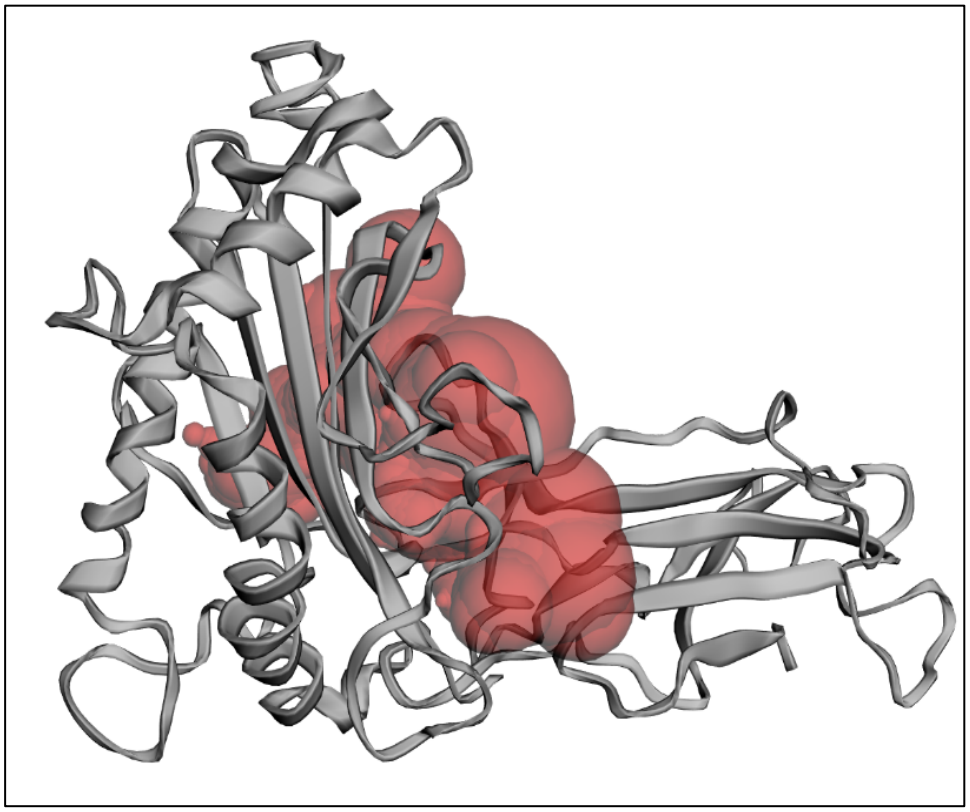

Figure 23. The figure displays the active site of the LYCAT protein computed by CASTp which contains following residues, MET1, SER3, TRP4, LYS5, GLY6, ILE7, PHE9, ILE10, LEU11, LEU13, SER21, PHE23, MET24, LEU25, PRO27, LEU29, PRO30, MET32, ASN35, LEU36, SER37, ARG40, SER43, ARG45, VAL47, 48ALA, THR49, TRP50, LEU51, PRO54, LYS112, SER114, LYS116, SER117, VAL118, PRO119, GLY120, PHE121, GLY122, TRP123, ALA124, MET125, ILE133, LYS136, TRP137, LYS138, ASP140, LYS141, SER142, PHE144, GLU156, HIS233, GLN282, GLY283, GLU284, ASN286, VAL307, LYS308, LEU309, SER311, ILE312, VAL313, PHE318, ALA321, MET322, CYS323, LEU324, ILE326, TYR327, LEU328, HIS365 and LYS366. A large number of these residues are functionally important

e. Studying binding interactions between modelled LYCAT structure and peptide inhibitor using HPEPDOCK-molecular docking:

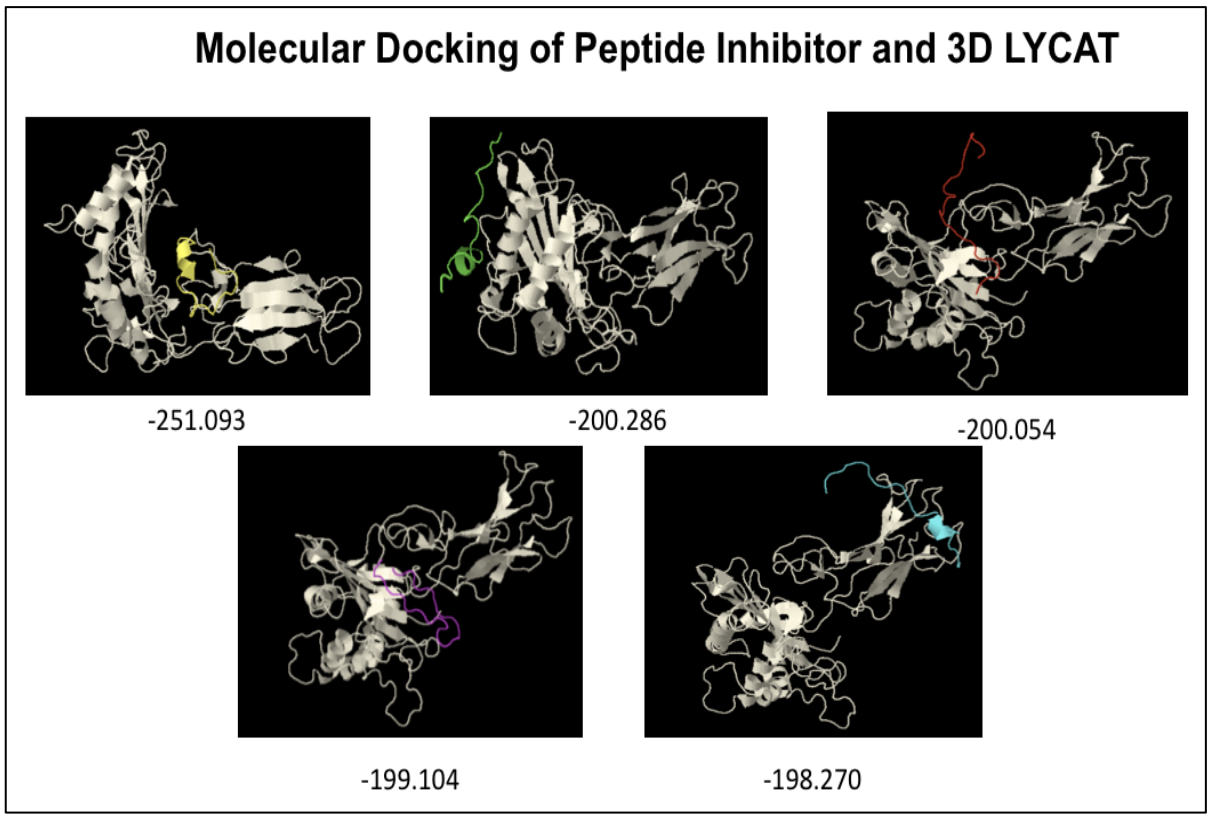

Figure 24. HPEPDOCK has generated multiple models when it docked LYCAT homology model with peptide inhibitor, among which five models are shown in the figure with their respective binding energies. The docked arrangement is in the order of their rank, the first one being the best docking model between the protein and peptide with -251.093 binding energy.

IV. DISCUSSIONS

The major findings of this project are, (i) Cigarette smoke extract enhances LYCAT protein and mRNA expressions in Bronchial epithelial cells. (ii) Cigarette smoke extract induced total and mitochondrial Reactive oxygen species in Beas2B cells is increased and inhibition of LYCAT with peptide mimetic attenuated total and mitochondrial ROS in CSE induced Beas2B cells. (iii) CSE induces apoptosis in Beas2B cells and blocking LYCAT with peptide mimetic reduces CSE induced apoptosis. (iv) Cardiolipin fatty acid composition is changed in CSE induced lipid extract when compared to controls while the lipid phosphorous of cardiolipin separated by TLC did not show any significant change between control and CSE lipid extracts. (v) The LYCAT activity was attenuated in LYCAT overexpressed Beas2B Cells in when treated with peptide mimetic. (vi) LYCAT homology model was build using MODELLER9.19 comparative modelling software. (vii) The active site of LYCAT homology model was determined using CASTp. (viii) Molecular docking was performed between peptide mimetic and LYCAT homology model using HPEPDOCK.

Cardiolipin plays an important role in apoptosis, electron transport chain and oxidative phosphorylation[31, 32]. Lipid peroxidation of cardiolipin and fatty acid composition leads to mitochondrial dysfunction in several disease models. Lipid peroxidation of CL occurs due to oxidative stress, causes de-acylation of CL followed by re-acylation by LYCAT. In our study we have demonstrated that inhibiting LYCAT is beneficial and protective for COPD.

This study demonstrates direct relationship between LYCAT expression, ROS and apoptosis.

Oxidative stress plays a key role in cigarette smoke extract induced pulmonary disorders, it is the predisposing factor in the pathogenesis of COPD[33]. Oxidants are produced in airways by cigarette smoking, as an antioxidant defense mechanism ROS is produced in excess. Therefore, it is important to understand the mechanisms underlying oxidative stress and develop novel therapies. In our *in vitro* study, we investigated that CSE enhanced mRNA and protein expression of LYCAT (Fig 5-6), we also determined that oxidative stress increases in Beas2B cells when treated with cigarette smoke extract, and LYCAT inhibition reduces the oxidative stress in epithelial cells, thus suggesting potential role of LYCAT against COPD (Fig 7-11).

Another important illustration of this project is to study the role of LYCAT expression against epithelial apoptosis in *in vitro* analysis. Apoptosis is also termed as programmed cell death, which is a tightly regulated mechanism. Apoptosis allows elimination of damaged, infected and unwanted cells[34]. Oxidative stress in the cells lead to cell dysfunction or cell death(apoptosis). In our study we demonstrated the role of CSE induced apoptosis in pathogenesis of COPD and concluded that cigarette smoke extract induced oxidative stress leads to apoptosis and blocking LYCAT with a peptide mimetic reduces oxidative stress and apoptosis. This concludes that, inhibiting LYCAT with peptide mimetic is protective against CSE induced apoptosis supported with flow cytometry and decreased caspase 3 cleavage (Fig 12).

The lipid extracts from control and cigarette smoke extract treated cells were subjected to 2-Dimensional Thin Layer chromatography and total lipid phosphorous was analyzed and there was no change in cardiolipin lipid phosphorous, but when the samples were subjected to GC-MS for determining the fatty acid composition, there was change in CSE lipid extracts

compared to control (Fig. 14). The C (18:1) fatty acid profile of CL in mitochondria was increased in control compared to CSE lipid extracts. This change is regulated by the enzyme LYCAT (Fig. 13-15).

In this study LYCAT expression was identified to be a potential target for COPD, which could be a promising therapeutic target. By using computer-assisted technology like homology modeling, LYCAT protein was designed. 1BD2 was identified as template, which showed 46% of identity with the query sequence (Fig. 16,17,18). MODELLER9.19 was used to develop the model, five best models were generated the one with least DOPE score was selected as the best model (Fig. 19). Later the model was further validated with SWISS structural assessment using Ramachandran plot and molecular docking. The Ramachandran plot revealed that the residues in the favored region was 84.76%, allowed region was 4.81% and outlier region was 4.97% residues respectively, among 376 amino acids 84.76% were in the favored region and the QMEAN and Z-scores were -11.19 and -0.94 respectively which were assessed using SWISSMODEL assessment and PROSA servers which suggested that the model is of better quality, and further refinement can be done using loop refinement of the homology model (Fig. 20,21,22).

The active site of LYCAT was assessed using CASTp server which predicts the surface topography. The volume and surface area of all the expected pockets and cavities on the 3D structure of LYCAT protein was measured, where the volume and surface area of largest pocket was 2029.864 $Å^2$ and 1417.854 $Å^3$ respectively, which is considered as the biological active site of LYCAT (Fig 23).

The molecular docking between LYCAT and peptide mimetic was performed using HPEPDOCK, which generated five top models, with their binding energies. The lowest docked energy is considered to be the best possible binding conformation. In our study, the lowest docking energy was -251.093 $Kcalmol^{-1}$ and the first binding model is the most probable model between peptide mimetic and LYCAT homology model (Fig.24).

In summary, these results conclude that cigarette smoke extract induced expression of LYCAT is not protective in COPD, as it leads to increase in total ROS, mitochondrial oxidative stress, apoptosis and changes fatty acid composition of cardiolipin, therefore blocking LYCAT with peptide mimetic reduces ROS and apoptosis which is beneficial in COPD. In order to further determine the role of LYCAT in COPD, developing the 3D structure and knowing the ligand receptor interactions is important in structure-based drug design, therefore a homology model was built and interactions between the model and mimetic were studied. The active site of the homology model of LYCAT was determined. Further, investigating the role of LYCAT expression and determining the structure-functional relation could provide a novel therapeutic strategy for Chronic Obstructive Pulmonary Disorder.

Future Directions

i. To further analyze, the role of LYCAT by blocking Mito-ROS using Mito tempo.
ii. To study the role of CSE induced LYCAT expression on antioxidant mechanism in development of COPD.

iii. To work on different cell types apart from Bronchial epithelial cells, to focus on the role of LYCAT in modulation between different cell types.

iv. To develop small molecule chemical inhibitors to target the active site of the LYCAT homology model which could be a potential therapeutic drug.

V. REFERENCES

1. Smith, M.C. and J.P. Wrobel, *Epidemiology and clinical impact of major comorbidities in patients with COPD.* Int J Chron Obstruct Pulmon Dis, 2014. **9**: p. 871-88.
2. Macklem, P.T., *The mechanics of breathing.* Am J Respir Crit Care Med, 1998. **157**(4 Pt 2): p. S88-94.
3. Forey, B.A., A.J. Thornton, and P.N. Lee, *Systematic review with meta-analysis of the epidemiological evidence relating smoking to COPD, chronic bronchitis and emphysema.* BMC Pulm Med, 2011. **11**: p. 36.
4. Santucci, R., et al., *Role of cardiolipin in mitochondrial diseases and apoptosis.* Curr Med Chem, 2014. **21**(23): p. 2702-14.
5. Flis, V.V. and G. Daum, *Lipid transport between the endoplasmic reticulum and mitochondria.* Cold Spring Harb Perspect Biol, 2013. **5**(6).
6. Lamari, F., F. Mochel, and J.M. Saudubray, *An overview of inborn errors of complex lipid biosynthesis and remodelling.* J Inherit Metab Dis, 2015. **38**(1): p. 3-18.
7. Xiong, J.W., et al., *An acyltransferase controls the generation of hematopoietic and endothelial lineages in zebrafish.* Circ Res, 2008. **102**(9): p. 1057-64.
8. Patan, S., *Lycat and cloche at the switch between blood vessel growth and differentiation?* Circ Res, 2008. **102**(9): p. 1005-7.
9. Wang, W., et al., *Expression of the Lycat gene in the mouse cardiovascular and female reproductive systems.* Dev Dyn, 2010. **239**(6): p. 1827-37.
10. Huang, L.S., et al., *Lysocardiolipin acyltransferase regulates TGF-beta mediated lung fibroblast differentiation.* Free Radic Biol Med, 2017. **112**: p. 162-173.
11. Huang, L.S., et al., *The mitochondrial cardiolipin remodeling enzyme lysocardiolipin acyltransferase is a novel target in pulmonary fibrosis.* Am J Respir Crit Care Med, 2014. **189**(11): p. 1402-15.
12. Nair, R., et al., *Structural genomics is the largest contributor of novel structural leverage.* J Struct Funct Genomics, 2009. **10**(2): p. 181-91.
13. R, S., J. J, and T.S. A, *Purification, characterization, molecular modeling and docking study of fish waste protease.* Int J Biol Macromol, 2018. **118**(Pt A): p. 569-583.
14. Vyas, V.K., et al., *Homology modeling a fast tool for drug discovery: current perspectives.* Indian J Pharm Sci, 2012. **74**(1): p. 1-17.
15. Camacho, C., et al., *BLAST+: architecture and applications.* BMC Bioinformatics, 2009. **10**: p. 421.
16. Pearson, W.R., *Finding Protein and Nucleotide Similarities with FASTA.* Curr Protoc Bioinformatics, 2016. **53**: p. 3 9 1-25.
17. Benkert, P., S.C. Tosatto, and D. Schomburg, *QMEAN: A comprehensive scoring function for model quality assessment.* Proteins, 2008. **71**(1): p. 261-77.
18. Wiederstein, M. and M.J. Sippl, *ProSA-web: interactive web service for the recognition of errors in three-dimensional structures of proteins.* Nucleic Acids Res, 2007. **35**(Web Server issue): p. W407-10.

19. Carugo, O. and K. Djinovic-Carugo, *A proteomic Ramachandran plot (PRplot).* Amino Acids, 2013. **44**(2): p. 781-90.
20. Allison, B., et al., *Computational design of protein-small molecule interfaces.* J Struct Biol, 2014. **185**(2): p. 193-202.
21. di Luccio, E. and P. Koehl, *A quality metric for homology modeling: the H-factor.* BMC Bioinformatics, 2011. **12**: p. 48.
22. Webb, B. and A. Sali, *Comparative Protein Structure Modeling Using MODELLER.* Curr Protoc Bioinformatics, 2014. **47**: p. 5 6 1-32.
23. Meng, X.Y., et al., *Molecular docking: a powerful approach for structure-based drug discovery.* Curr Comput Aided Drug Des, 2011. **7**(2): p. 146-57.
24. Tanchuk, V.Y., et al., *A New Scoring Function for Molecular Docking Based on AutoDock and AutoDock Vina.* Curr Drug Discov Technol, 2015. **12**(3): p. 170-8.
25. Tripathi, A. and V.A. Bankaitis, *Molecular Docking: From Lock and Key to Combination Lock.* J Mol Med Clin Appl, 2017. **2**(1).
26. Wu, L., et al., *Homology modeling and molecular docking of human pituitary adenylate cyclaseactivating polypeptide I receptor.* Mol Med Rep, 2014. **10**(4): p. 1691-6.
27. Shen, M.Y. and A. Sali, *Statistical potential for assessment and prediction of protein structures.* Protein Sci, 2006. **15**(11): p. 2507-24.
28. Zhao, M.L., et al., *In silico structure prediction and inhibition mechanism studies of AtHDA14 as revealed by homology modeling, docking, molecular dynamics simulation.* Comput Biol Chem, 2018. **75**: p. 120-130.
29. Zhou, P., et al., *Hierarchical Flexible Peptide Docking by Conformer Generation and Ensemble Docking of Peptides.* J Chem Inf Model, 2018. **58**(6): p. 1292-1302.
30. Binkowski, T.A., S. Naghibzadeh, and J. Liang, *CASTp: Computed Atlas of Surface Topography of proteins.* Nucleic Acids Res, 2003. **31**(13): p. 3352-5.
31. Li, X.X., et al., *Cardiolipin and its different properties in mitophagy and apoptosis.* J Histochem Cytochem, 2015. **63**(5): p. 301-11.
32. Ren, M., C.K. Phoon, and M. Schlame, *Metabolism and function of mitochondrial cardiolipin.* Prog Lipid Res, 2014. **55**: p. 1-16.
33. Maltais, F., et al., *An official American Thoracic Society/European Respiratory Society statement: update on limb muscle dysfunction in chronic obstructive pulmonary disease.* Am J Respir Crit Care Med, 2014. **189**(9): p. e15-62.
34. Gogebakan, B., et al., *The role of bronchial epithelial cell apoptosis in the pathogenesis of COPD.* Mol Biol Rep, 2014. **41**(8): p. 5321-7.

VI. CURRICULUM VITAE

MOUNICA BANDELA

Educational Qualifications

The University of Illinois at Chicago (UIC) – Chicago, IL — **July 2018**
Master of Science in Bioengineering — GPA: 4.0/4.0

Osmania University – Hyderabad, India — **June 2016**
Diploma in Bioinformatics — GPA: 4.0/4.0

Osmania University – Hyderabad, India — **May 2015**
Bachelor of Technology in Biotechnology — GPA: 4.0/4.0

Research Experience

Department of Pharmacology-UIC — **April 2017 - July 2018**
Research Assistant

Department of Biological Sciences-UIC — **Jan 2017 – Present**
Graduate Teaching Assistant

Department of Microbiology and Immunology-UIC — **Oct 2016 – Aug 2017**
Laboratory Aide

Department of Microbiology-Sir Ronald Ross Institute of Tropical and Communicable Diseases, Osmania General Hospital — **Aug 2014 – May 2015**
Research Trainee

Clinical Biochemistry Laboratory – Osmania General Hospital — **May 2014-July 2014**
Summer Intern

Publications

1. Mantri, Neelamma, Jaheer Mohmed, Seshagiri Bandi, G. H. Anuradha, and **Mounica Bandela**. "CoMFA, CoMSIA analysis of 4-[5-(4-Fluoro-benzyl-1H-pyrazol-3-yl]-pyridine derivatives as CYP3A4 inhibitors." *International Journal of Computational Biology and Drug Design* 10, no. 3 (2017): 225-236.
2. Kashetty, Sandeep Kumar, **Mounica Bandela**, Uday Kanth Suryavanshi, and Vijayalakshmi Lokirevu. "In silico Modelling and Docking Studies of Camptothecin Derivatives." *International Journal of ChemTech Reaseach9*, no 09 (2016): 274-284.
3. Abhigna, P., **Mounica Bandela**, Sandeep Kumar Kashetty, and Mahmood Shaik. "In silico modelling and docking studies of natural flavonoid derivatives as tetanus inhibitors." *International Journal of Research in Pharmaceutical Sciences*7, no. 3 (2017): 208-214.

Leadership Experience

Department of Bioengineering – UIC — **Aug 2016- May 2018**
Editor in Chief
UIC Bioengineering Student Journal (UBSJ)

Graduate Student Council (GSC) – UIC **Aug 2017- May 2018**
Student representative for Bioengineering department

Department of Biotechnology – Osmania University **June 2012 – May 2015**
Student Representative

Awards and Academic achievements

- Member of **Alpha Eta Mu Beta** an International Biomedical Engineering Honor Society, for earning high GPA of 4/4 during 2016-2018 at UIC.
- Recognized by "**Chancellor's Student Service and Leadership Award**", for voluntary services to GSC and UBSJ - April 2018, UIC.
- Awarded "**Academic excellence**" for securing highest marks in Biotechnology Department, Osmania University, as an undergraduate, 2012-2015.
- Awarded "**Most Regular Student Award**" for maintaining more than 90% of attendance during undergraduate, 2011-2015.

Workshops

- **"**Stem Cell Therapy", Technozion-Annual technical fest, National Institute of Technology, Warangal.
- "Current Trends in Nanotechnology", Technical Fest. Birla Institute of Technology, Hyderabad.

Campus Placements

Received offer from Accenture, Cognizant Technological Solutions and Infosys during pursuing undergraduate.